UNIVERSITY OF SOUTHERN CALIFORNIA
Department of Civil Engineering

NON-LINEAR EARTHQUAKE WAVES IN SEVEN-STOREY REINFORCED CONCRETE HOTEL

by

Vlado Gicev and Mihailo D. Trifunac

Report CE 06-03

November, 2006
Los Angeles, California

http://www.usc.edu/dept/civil_eng/Earthquake_eng/

ABSTRACT

The seven-story reinforced concrete building studied in this work was damaged during the 1994 Northridge, California earthquake. The damage was widespread but was mostly concentrated in the columns on the fourth floor, below the spandrel beam and the floor slab on the fifth floor. We show that such a concentration of damage can be explained by interference of non-linear waves in the building resulting from incident, upward-propagating earthquake pulses and downward propagation of pulses reflected from the roof of the building. We conclude that the analysis and prediction of where the localized damage may occur and the proper design to minimize and control such damage can be carried out best by non-linear wave propagation methods.

1. INTRODUCTION

The seven-story hotel building in Van Nuys, California (VN7SH) is becoming one of the most studied buildings in southern California. Many aspects of its response and damage, first during San Fernando, 1971, earthquake, and then the Northridge earthquake in 1994, have been examined. The relative simplicity, uniformity, and symmetry of its geometry make this building ideal for testing and for calibration of different analysis methods. So far, it has been difficult to explain why the main damage during the Northridge earthquake occurred in the fourth floor columns rather than at its base or throughout the structure.

In a study of the propagation of non-linear waves in a simple, uniform shear beam, caused by incident strong motion pulses, Gicev and Trifunac (2006) found that for large ground displacement pulses the maximum permanent strains in the beam occur mainly at the interface of the beam with the soil, while for smaller amplitudes of pulses permanent trains occur closer to the top of the beam. They identified three zones of the permanently deformed beam: (1) a permanently deformed zone at the bottom; (2) an intermediate zone, which is not deformed at its bottom part and is deformed in the top part; and (3) a non-deformed zone at the top of the beam. They found that the occurrence and the development of these zones depends upon the dimensionless excitation amplitudes and the dimensionless frequency of the incident strong motion pulses, and in particular on the conditions that lead to the occurrence of the first permanent strain. For large and long strong-motion pulses, only zones 1 and 3 are present in the beam. For large amplitudes and short strong-motion pulses, all three zones can develop and are present. For smaller excitation amplitudes only zones 2 and 3 exist in the beam.

Gicev and Trifunac (2006) further show that for excitation by near-field displacement pulses, failure can occur anywhere in the building, before the incident wave has completed its first travel from the foundation to the top of the building and back to the foundation. Because this travel time is shorter (by one half) than the natural period of the structure on the fixed base, it is seen that the common response spectrum method of analysis (based on the vibrational formulation of the solution) cannot provide the required details for the design of structures for such excitation. They noted that “to the extent that the locations of the plastic deformation zones can be controlled by the design process, absorption of the incident wave energy by structural members may become a new and powerful tool for performance-based design. To take advantage of such possibilities, the governing differential equations must be solved by the wave propagation method.”

The purpose of this work is to show that if the excitation is viewed as plane waves entering the beam (structure) vertically, the interference of the waves propagating up, and their reflection off the stress-free roof, can explain well the observed concentration of damage in VN7SH. Our approach in this work belongs to a group of wave propagation methods (Kanai 1965; Todorovska and Trifunac 2006a,b,c) and is also suitable for structural health monitoring and for real-time damage detection.

To minimize the consequences of rocking associated with soil-structure interaction and the contribution of torsion, in this work we analyze the EW (longitudinal) response of the VN7SH building only. The reader should be aware that ignoring the rocking contribution to the overall EW response will tend to make our model and the results similar to many engineering studies of this building, which typically ignore soil-structure interaction—that is, they assume that the building is supported by rigid soil. We will address the two- and three-dimensional aspects of this problem and the role of soil-structure interaction in our future work.

2. THE BUILDING

The building studied in this work is a seven-story hotel (VN7SH) located in Van Nuys, California. It was damaged by the 1994 Northridge, California earthquake (Ivanović et al. 1999a,b, Trifunac and Hao 2001, Trifunac et al. 1999a,b). Its response has been described and analyzed in numerous papers and reports.

The VN7SH (Fig. 1) is located in the central San Fernando Valley of the Los Angeles metropolitan area (at 34.221^{o} N and 118.471^{o} W). The building was designed in 1965, and constructed in 1966 (Blume and Assoc. 1973, Mulhern and Maley 1973, Table 2.1). Figure 2 shows a plan view of a typical floor (a), and a side view of the building frame (b). The building is 18.9 × 45.7 m in plan. The typical framing consists of columns spaced on 6.1 m centers in the transverse direction and 5.8 m centers in the longitudinal direction. Spandrel beams surround the perimeter of the structure.

Lateral forces in the longitudinal (EW) direction are resisted by interior column-slab frames and exterior column spandrel beam frames. The added stiffness in the exterior frames associated with the spandrel beams creates exterior frames that are roughly twice as stiff as interior frames. The floor system is reinforced concrete flat slab, 25.4 cm thick at the second floor, 21.6 cm thick at the third to seventh floors, and 20.3 cm thick at the roof (Browning et al. 2000, De La Llera at al. 2001, Islam 1996, Li and Jirsa 1998, Trifunac and Ivanović 2003).

Fig. 1. View of Van Nuys Seven Story Hotel (VN7SH) from North-East.

The building is situated on undifferentiated Holocene alluvium, uncemented and unconsolidated, with a thickness of < 30 m, and an age of < 10,000 years (Trifunac and Todorovska 1998). The average shear-wave velocity in the top 30 m of soil is 300 m/s, and the soil-boring log shows that the underlying soil consists primarily of fine sandy silts and silty fine sands. The foundation system consists of 96.5-cm deep pile caps, supported by groups of two to four poured-in-place 61-cm-diameter reinforced concrete friction piles. These are centered under the main building columns. All of the pile caps are connected by a grid of beams. Each pile is roughly 12.2 m long and has a design capacity of over 444.82×10^3 N vertical load and up to 88.96×10^3 N lateral load. The structure is constructed of normal-weight reinforced concrete (Blume and Assoc. 1973; Table 2.1).

Earthquake Damage. The M_L = 6.4 Northridge earthquake of January 17, 1994 severely damaged the building. The structural damage was extensive in the exterior north (D) and south (A) frames that were designed to take most of the lateral load in the longitudinal (EW) direction. Severe shear cracks occurred at the middle columns of frame A, near the contact with the spandrel beam of the 5th floor (Figs. 3 and 4). Those cracks significantly decreased the axial, moment, and shear capacity of the columns. The shear cracks that appeared in the north (D)

Table 2.1 Properties of the construction materials of the VN7SH building

Concrete (regular weight, 150 pcf [1])		
Location in the structure	Minimum specified compressive strength f_c' – psi [2]	Modulus of elasticity E – psi [2]
Columns, 1st to 2nd floors	5,000	4.2×10^6
Columns, 2nd to 3rd floors	4,000	3.7×10^6
Beams and slabs, 2nd floor	4,000	3.7×10^6
All other concrete, 3rd floor to roof	3,000	3.3×10^6

Reinforcing steel			
Location in the structure	Grade	Minimum specified yield strength f_y – ksi [3]	Modulus of elasticity E – psi [2]
Beams and slabs	Intermediate grade deformed billet bars (ASTM A-15 and A-305)	40	29×10^6
Column bars	Deformed billet bars (ASTM A-432)	60	29×10^6

[1] Pounds per cubic foot
[2] Pounds per square inch
[3] Kips per square inch

frame on the 3rd and 4th floors and the damage to columns D2, D3, and D4 on the 1st floor caused minor to moderate changes in the capacities of these structural elements. No major damage to the interior longitudinal (B and C) frames was observed, and there was no visible damage to the slabs or around the foundation. The nonstructural damage was also significant. The recorded peak accelerations in the building were 0.46g (L), 0.40g (T), and 0.28g (V) at the base, and 0.59g (L) and 0.58g (T) at the roof, along the longitudinal (L), transverse (T), and vertical (V) axes of symmetry (there were no sensors installed on the roof to measure vertical motions) (Trifunac et al 1999b).

Photographs and detailed descriptions of the damage from the earthquake can be found in Trifunac et al. (1999b) and Trifunac and Hao (2001). Analysis of the relationship between the observed damage and the changes in equivalent vertical shear-wave velocity in the building can be found in Ivanović et al. (1999b), and Todorovska and Trifunac (2006d). A discussion of the

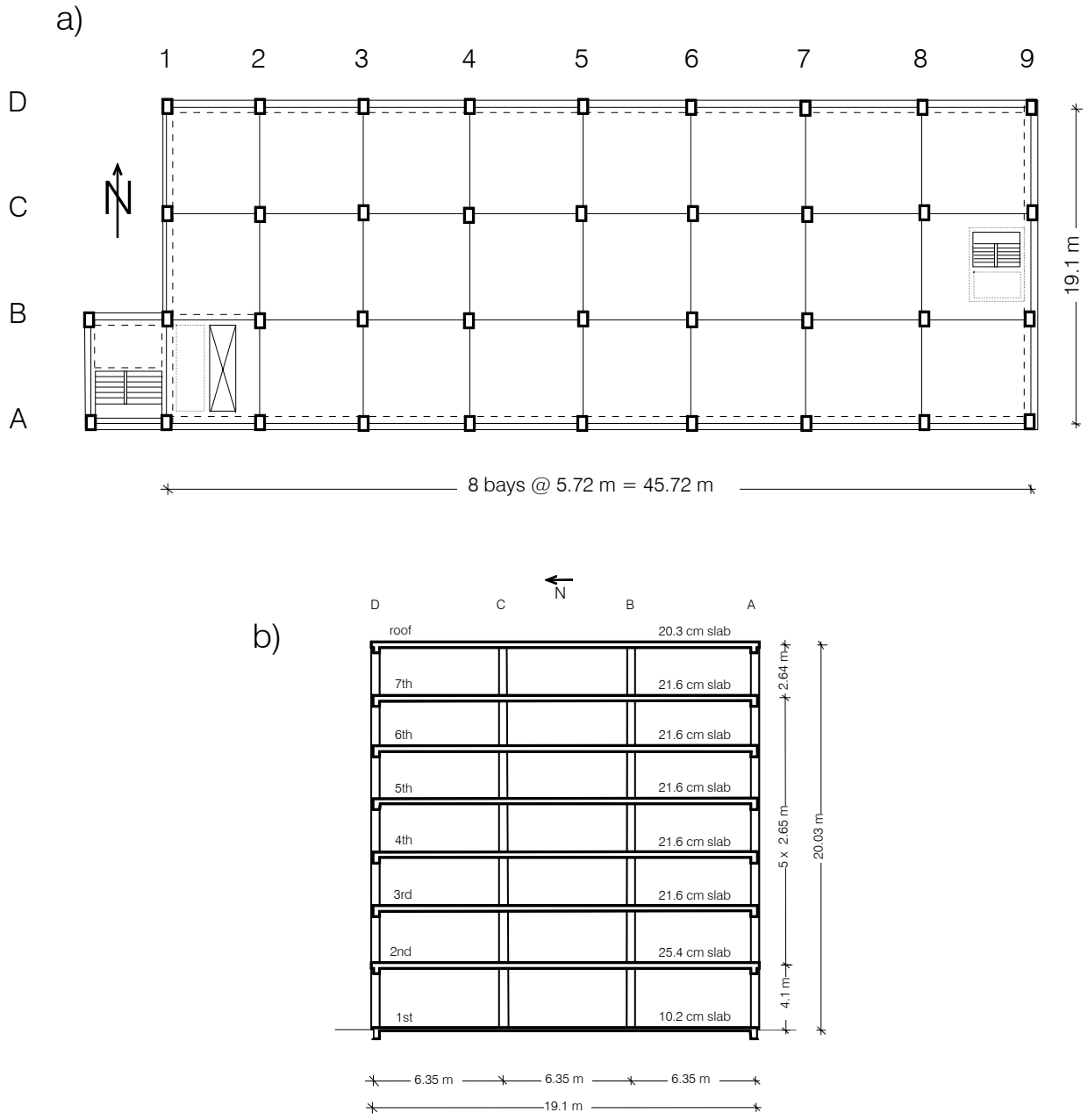

Fig. 2. Typical Floor Plan (a), and North-South section (b).

extent to which this damage has contributed to the changes in the apparent period of the soil-structure system can be found in Trifunac et al. [2001a,b].

Strong-Motion Records. The response of VN7SH was recorded by a 13-channel CR-1 central recording system and by one tri-component SMA-1 accelerograph, with an independent recording system but with common trigger time with the CR-1 recorder (Trifunac et al. 1999b).

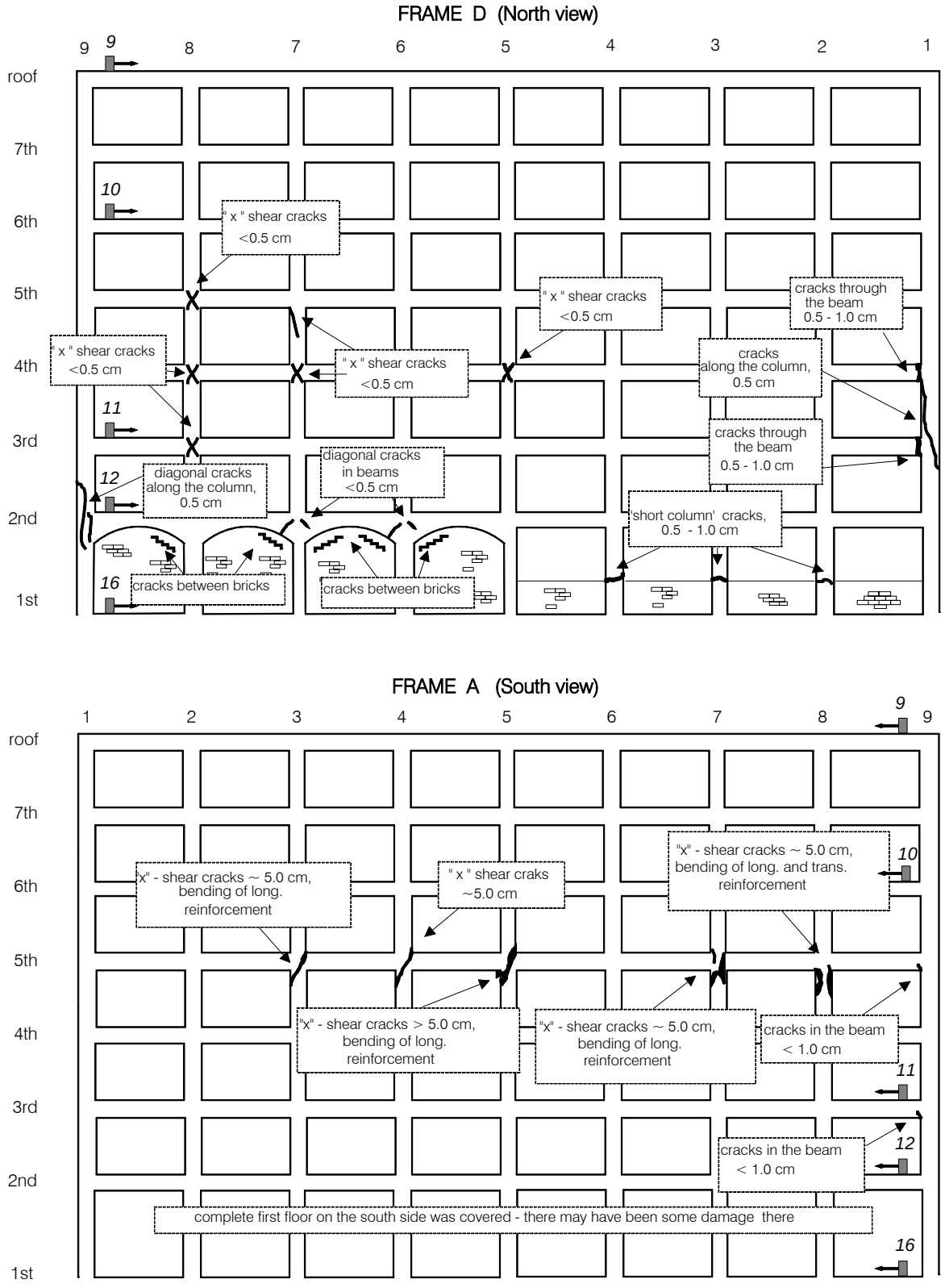

Fig. 3. Observed Damage of frames D (top) and A (bottom).

The locations of the five transducers, which recorded EW response of the building during earthquake, is shown in Fig. 3.

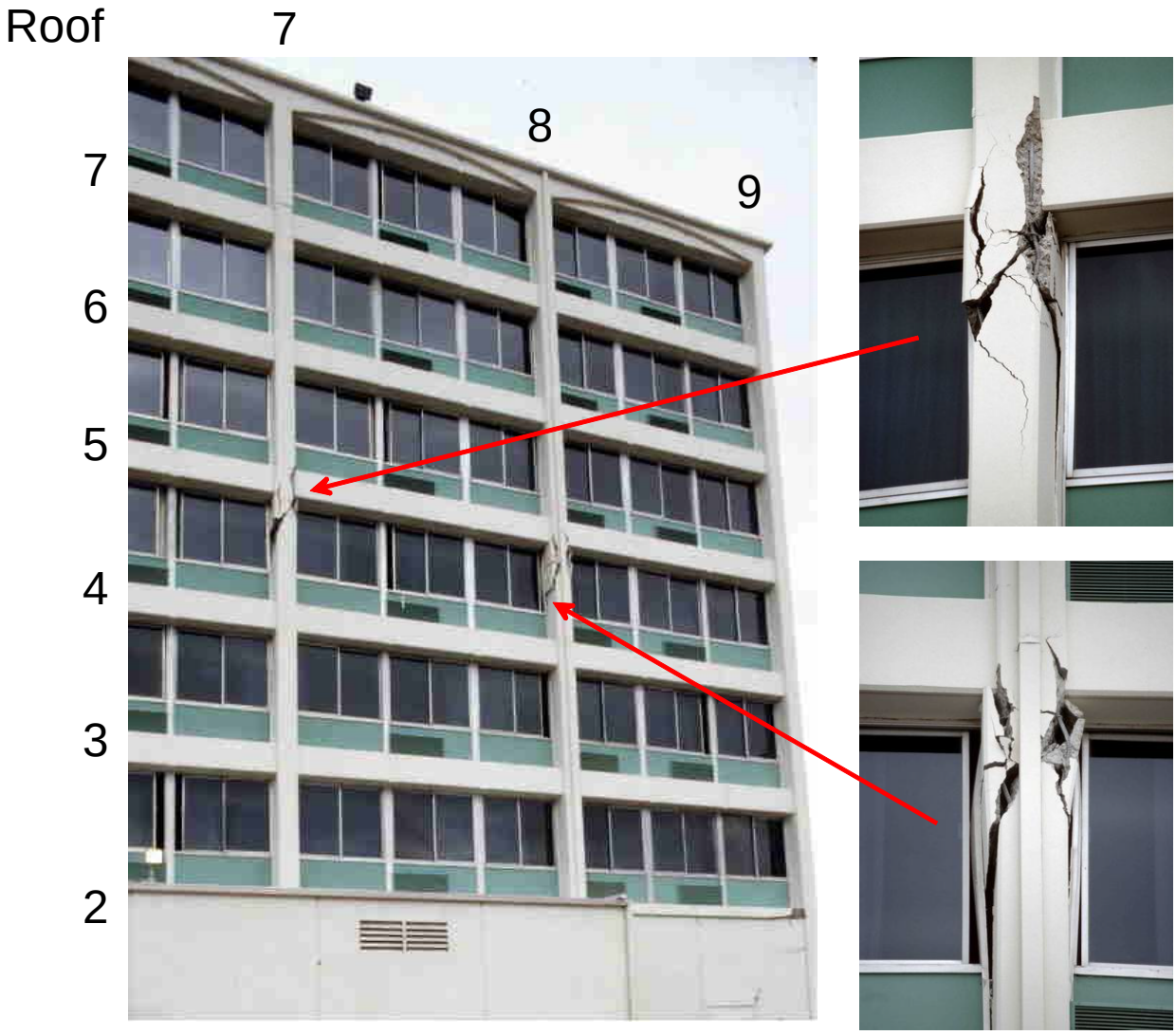

Fig. 4. Post-earthquake view of damaged columns A7 and A8.

3. PREVIOUS WORK

Since 1994, the VN7SH building has emerged as a useful benchmark for comparison of different analyses. Trifunac et al. (1999b) and Trifunac and Hao (2001) presented photographs of the damage following the earthquake and collected all of the strong-motion data digitized thus far for the period between 1971 and 1994. Two full-scale ambient vibration tests were performed

(Ivanović et al., 1999a; 2000). During the second ambient vibration survey, measurements of wave motion through the building foundation showed that the foundation is "flexible" and deforms with the passage of micro-tremor waves, which indicates that for studies of soil-structure interaction the rigid foundation assumption may not be appropriate (Trifunac et al., 1999a). The apparent period of the soil-structure system and its dependence upon the response amplitudes in VN7SH were described by Trifunac et al. (2001a,b), and an application of off-line and on-line identification techniques to the building response data in VN7SH was presented by Loh and Lin (1996). A continuum mechanics representation of VN7SH was considered in terms of isotropic and anisotropic two-dimensional models and their response to incident wave motion by Todorovska et al. (2001a,b). The feasibility of identifying the observed damage through wave propagation studies using recorded earthquake responses was explored in Ivanović et al. (1999b) and Trifunac et al. (2003). The accounting of incident-wave energy, its redistribution among different response energies, and the power of incident-wave motion and its capacity to damage the VN7SH structure has been described in Trifunac et al. (2001c).

The engineering studies of VN7SH have focused mainly on its longitudinal (EW) response. Without exception, these studies have neglected the effect of soil-structure interaction and have implicitly assumed that all non-linearities in the observed response are associated with the building structure.

Islam (1996) considered two two-dimensional models for EW response of the building, one with and one without the brick infill walls in the four bays of the northern perimeter frame D (see Figs. 1 and 3). Assuming the building to be fixed at the ground floor level, he used the triangular distributed horizontal load to perform a push-over analysis. Figure 5 shows his results for V/W, the resulting base shear (V), normalized by the appropriate fraction of building weight (W), versus roof displacement, assuming that the south perimeter frame (A) resists one third of the lateral load. Figure 6 shows the story drifts calculated by Islam, using *elastic time history* analysis, at the center of mass (COM), the NE corner, and the SW corner, for the two models, with and without the infill walls in frame D. For comparison, we also show in this figure the "observed" drift amplitudes, evaluated on February 4, 1994, based on detailed analysis of the cracks, the scratches caused by relative motion on the partition walls, and the marks on the interior appearance of the perimeter walls (Trifunac and Ivanović 2003). Islam concluded that "many of the structural elements may have exceeded their elastic limit state at approximately 4 seconds into the earthquake. However, the most severe damage—e.g., breakdown of the entire load path in the south perimeter frame columns immediately below the 5th floor level—may have actually occurred at approximately 9 seconds, which coincides with the time of the peak ground acceleration in the longitudinal direction." He also notes that "a push-over analysis performed on the longitudinal frame with a triangular load pattern was unable to predict the damage observed in the building."

Li and Jirsa (1998) performed a *non-linear time history* analysis of VN7SH in the longitudinal (EW) direction "only because most of the damage occurred in this direction." Acceleration time histories recorded at ground level were used as input ground motion, and columns were assumed to be fixed at the base. Soil-structure interaction was not included in

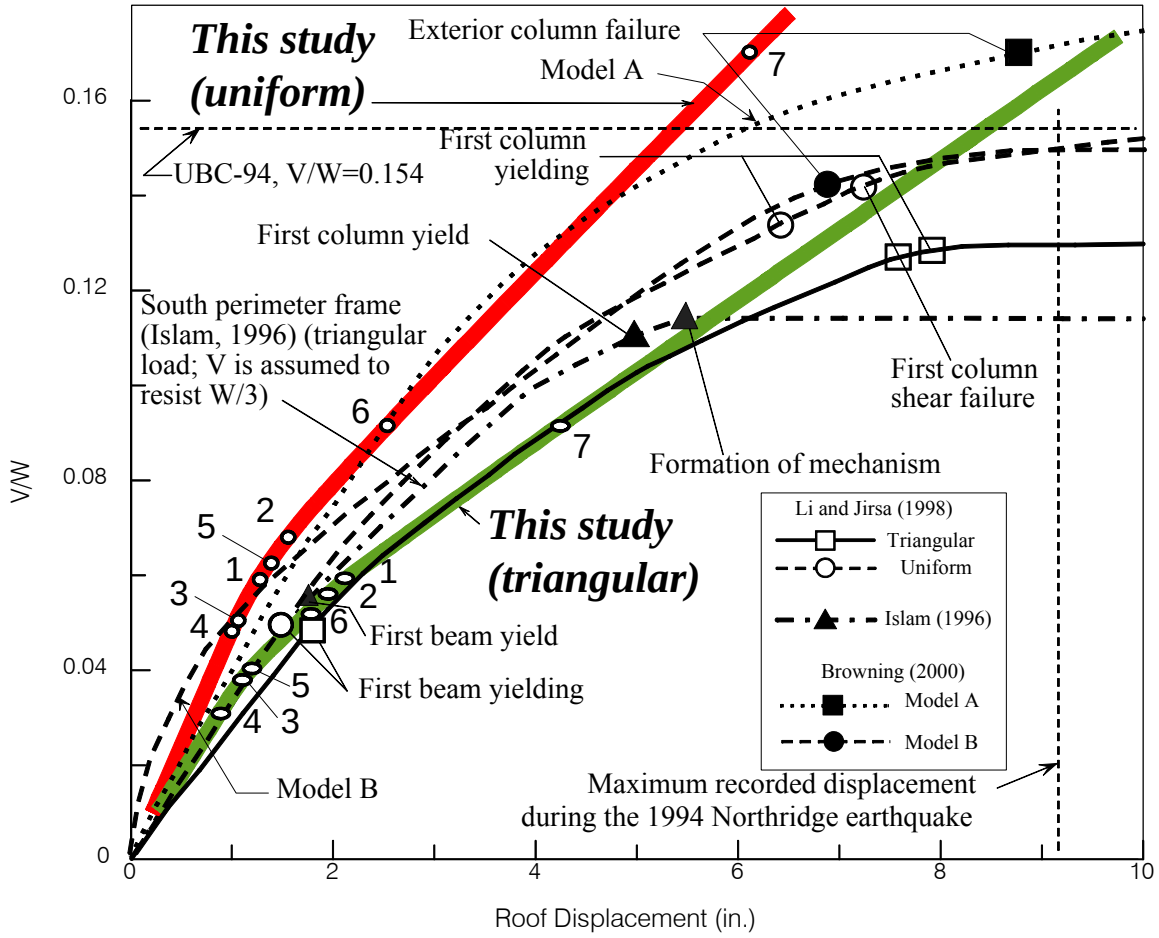

Fig. 5. Base shear (V) coefficient normalized by total building weight, W, versus EW roof displacement of VN7SH (*This study;* Islam, 1996; Li and Jirsa, 1998; and Browning et al, 2000: Models A and B).

the models. Effective stiffness and residual lateral capacity were chosen so that the period of calculated response-time history would match the recorded time history, and 0.35 EI_g was chosen as an effective stiffness for all beams and columns. Their analysis was two-dimensional, and therefore no torsional effects of excitation and of response could be included. Calculated maximum drift ratios from Li and Jirsa (1998) are reproduced in Figure 6, where they can be compared with other drift estimates. The authors interpreted their results to indicate that "the building was very close to collapse. Therefore, the drift limit recommended by NEHRP-94 appears to be reasonable … as a life safety limit for this structure." While describing their push-

over analysis (see Fig. 5), Li and Jirsa stated that "Push-over analysis successfully predicted that the structure almost lost its lateral load-resisting capacity, and the shear failures of columns occurred prior to reaching the maximum roof displacement the building experienced during the earthquake."

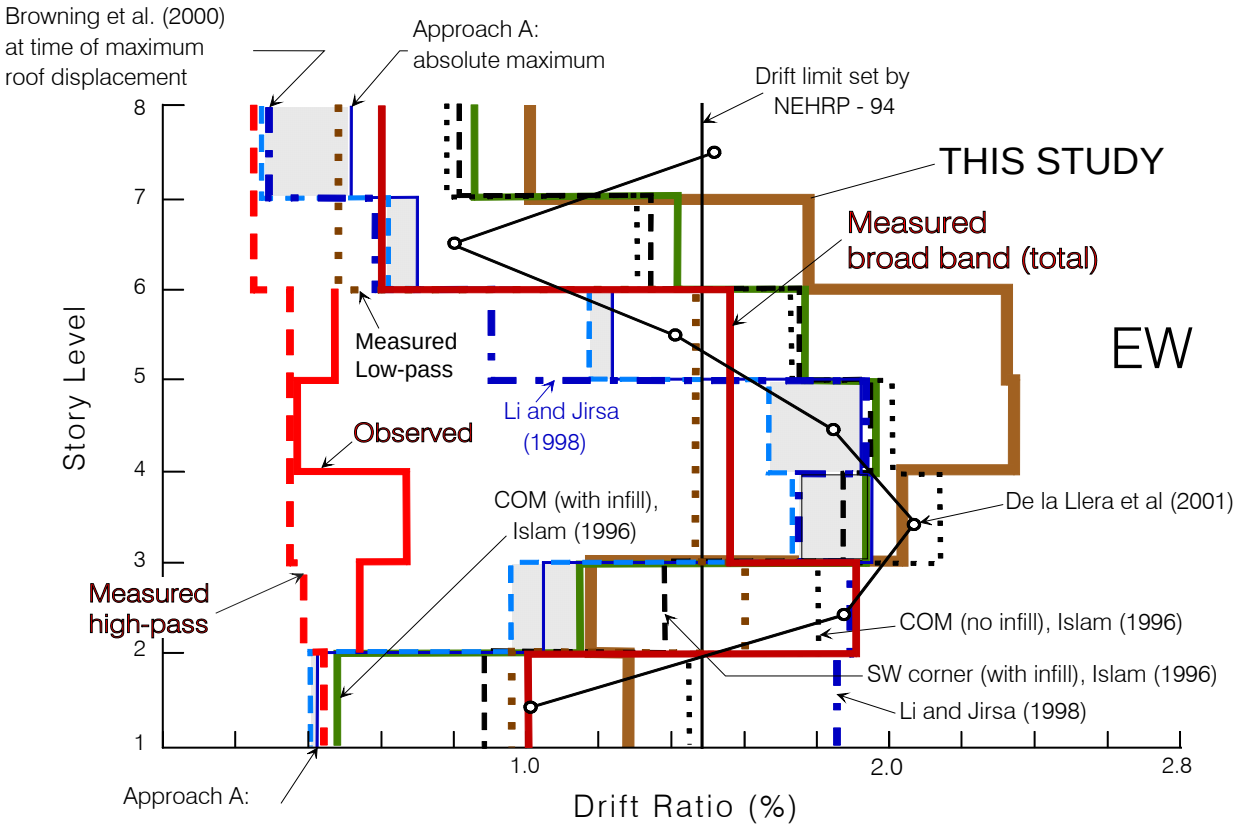

Fig. 6. Comparison of different estimates of EW drift in VN7SH during 1994 Northridge earthquake.

Browning et al. (2000) compared three independent analyses, including their own results, with regard to the response of VN7SH to the Northridge earthquake: Approach A (by Lynn and Moehle); Approach B (by Browning and Sozen); and Approach C (by Li and Jirsa). Because approach C has already been summarized, we will describe briefly only the results of the analyses based on approaches A and B. ***Approach A*** idealizes the building as a two-dimensional frame and considers only longitudinal (interior and exterior) framing lines. A simple bi-linear relation without stiffness or strength degradation is used to describe load deformation properties of the frames. The foundation is assumed to be rigid—that is, no soil-structure interaction is considered, and the authors used triangular load distribution with monotonically increasing amplitude in their push-over analysis (Fig. 5). Dynamic *non-linear response histories* were computed for the motion measured at the base of the building, and drift amplitudes were

computed (1) at the time of maximum roof response, and (2) using absolute maxima of drift over time. The range between these two estimates is shown as the gray zone in Fig. 6. ***Approach B*** used a model geometry similar to that of model A, but the in-fill was assumed not to contribute to resistance to the lateral forces. A *Takeda non-linear model* with unloading stiffness reduction equal to 0.4 was adopted, and non-linear static and dynamic response analyses were conducted. The results of the push-over analysis are shown in Fig. 5. *Approach A* gives smaller drift between the first and second floors relative to all other drift predictions shown in Fig. 6. Between the third and fifth floors, it is in excellent agreement with the drifts predicted by Li and Jirsa (1993) and Islam (1996).

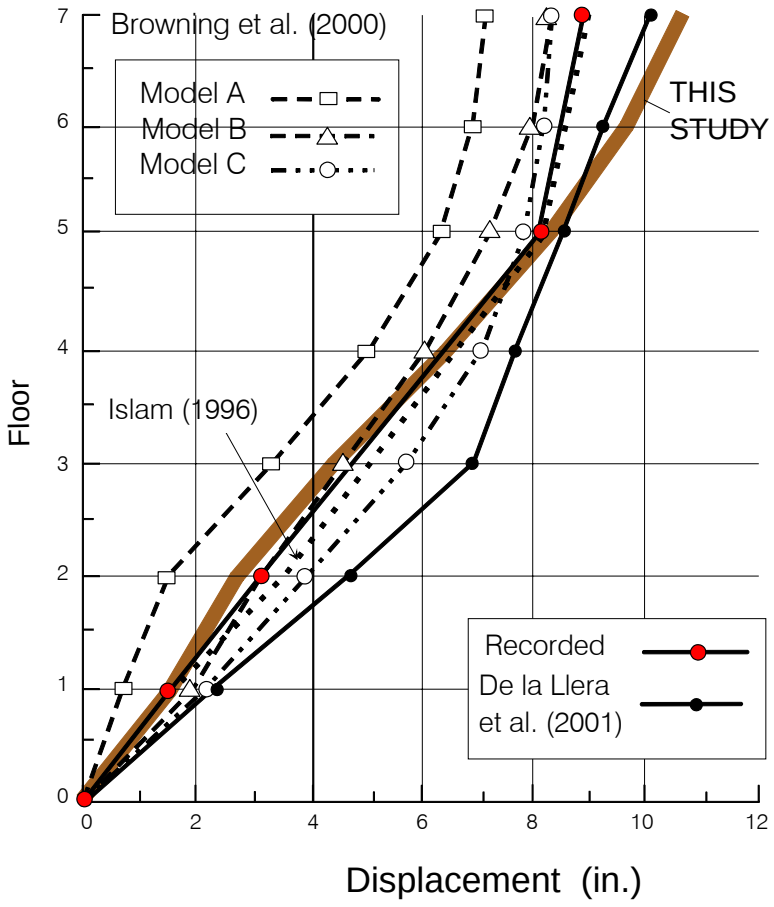

Fig. 7. Comparison of recorded and calculated maximum floor displacements in VN7SH during the Northridge 1994 earthquake.

De la Llera et al. (2002) noted that "planar analyses of the building reported previously are obviously not capable of predicting… torsional motion." They developed an idealization of the building consisting of a "single column-like element" (SEM) connecting two consecutive floors

and used this model to interpret the three-dimensional response of the VN7SH building to the earthquake. Their estimates of the envelopes of maximum floor drifts are shown in Fig. 6, and their estimates of maximum floor displacements using the single-element model are compared in Fig. 7 with recorded and other calculated relative displacements at the time of maximum response. Their estimates of EW (longitudinal) drifts are in fair agreement with the corresponding estimates of Islam (1996). As in all previous investigations of the response of this building, De la Llera et al. (2001) ignored soil-structure interaction effects in their analyses of translational and torsional responses. They interpreted the recorded motions to show that the "maximum acceleration along plane A (or D) due to torsion is 0.12 g, which is about 40% of that due to translation." Because the building is symmetric, De la Llera et al. (2001) concluded that "these significant torsional motions must be attributed primarily to the yielding of the structure, predominantly in one resisting plane (plane A)…." That is, they expressed the belief that these significant torsional motions began at about 4 s into the recorded strong motion during the earthquake and that they were followed by another episode of large rotations starting at about 7.5 s, the time when most of the damage occurred. Perusal of the analysis of drifts in this building (Trifunac and Ivanović 2003) will show, however, that the relative torsional response was prominent during all previous recorded responses in this building, as was the case during the Whittier 1987, Landers 1992, and Big Bear 1992 earthquakes, when the VN7SH building experienced no damage. Thus, while the eccentricity caused by damage must have contributed to the coupling of translational and torsional responses during the Northridge earthquake (Trifunac et al., 1999b), thus increasing the relative torsional response, the bulk of the observed torsional response appears to have resulted from the wave-passage effects alone (Todorovska et al., 2001a,b).

4. ONE-DIMENSIONAL WAVE-PROPAGATION MODEL

The location of the instruments that recorded the EW response is shown in Fig. 3. To search for the model parameters, we calculate the EW response of the building by assuming that the driving motion can be approximated by strong motion recorded at the basement (channel 16) and then comparing the results with the recorded motions at higher floors in the building (channel 12 at the first floor, channel 11 at the second floor, channel 10 at the fifth floor, and channel 09 at the roof).

The assumption that the foundation moves according to the recorded displacement at the location of channel 16 is equivalent to assuming that (1) ground is rigid, (2) there is no soil-structure interaction, and (3) all wave energy created by the motion of the base (ground floor) is trapped inside the building. These assumptions are analogous to what many previous investigators assumed in the analyses of the response of this building (Islam 1996, Li and Jirsa 1993,

Browning et al. 2000, De la Llera et al. 2002), but they are physically not correct. Under ideal conditions, if one could select a building model that would delay and modify the waves propagating up and down the building, exactly as would the real building, the phase of the down-propagating waves would be correct, and the motion would interfere with the driving displacement of the ground floor, exactly as this would occur in the presence of flexible soil, with soil-structure interaction, and with the transparent boundary at the base, allowing the down-propagating waves to be transmitted into the half space. Our model will not be able to achieve all of this, however, and therefore our analysis is only approximate.

The one-dimensional model we chose for this analysis consists of fourteen layers representing seven floors, with dimensions (thickness) of the layers h(i), velocities of shear waves $\beta(i)$, and material densities $\rho(i)$, for $1 \le i \le 14$, where $i = 2k-1 (k = 1,2,..,7)$ represent inter-story space ("soft" layers), and $i = 2k$ $(k = 1,2,..,7)$ represent floor slabs ("hard" layers) (see Table 4.1). The velocity of shear waves and the density of the layers we adopted for this work are based on the analysis of the impulse response for EW recorded motions in VN7SH (Todorovska and Trifunac 2006d). As can be seen from Table 4.1, the stiffness of the floor slabs is much larger than the stiffness of the inter-story space, so it can be expected that the floors will move with little elastic deformation and negligible contribution to drift.

We assume the bi-linear constitutive law $\sigma = \sigma(\varepsilon)$, where σ is shear stress and ε is shear strain at a grid point (Fig. 8). The first slope, μ_{0b}, represents the linear (initial) shear modulus, while the second slope, $\mu_{1b} = \gamma\mu_{0b}$, represents the shear modulus after yielding. The yielding strain in the building is ε_{yb}.

The points at the contacts between the layers are assumed to be in a linear state. To maintain the continuity of the displacements and stresses at the contacts between the layers, we introduce the equivalent shear moduli at the contact point i as

$$\mu_{ci} = \frac{\mu_{0b(i+1)}\mu_{0b(i-1)}\left(\Delta x_{i+1} + \Delta x_{i-1}\right)}{\mu_{0b(i+1)}\Delta x_{i-1} + \mu_{0b(i-1)}\Delta x_{i+1}}, \qquad (4.1)$$

where $\mu_{ob(i+1)}$ and $\mu_{ob(i-1)}$ are initial shear moduli of the layers above and below the contact point i, Δx_{i+1} and Δx_{i-1} are the spatial intervals above and below, and μ_{ci} is the initial equivalent shear modulus of the contact point i.

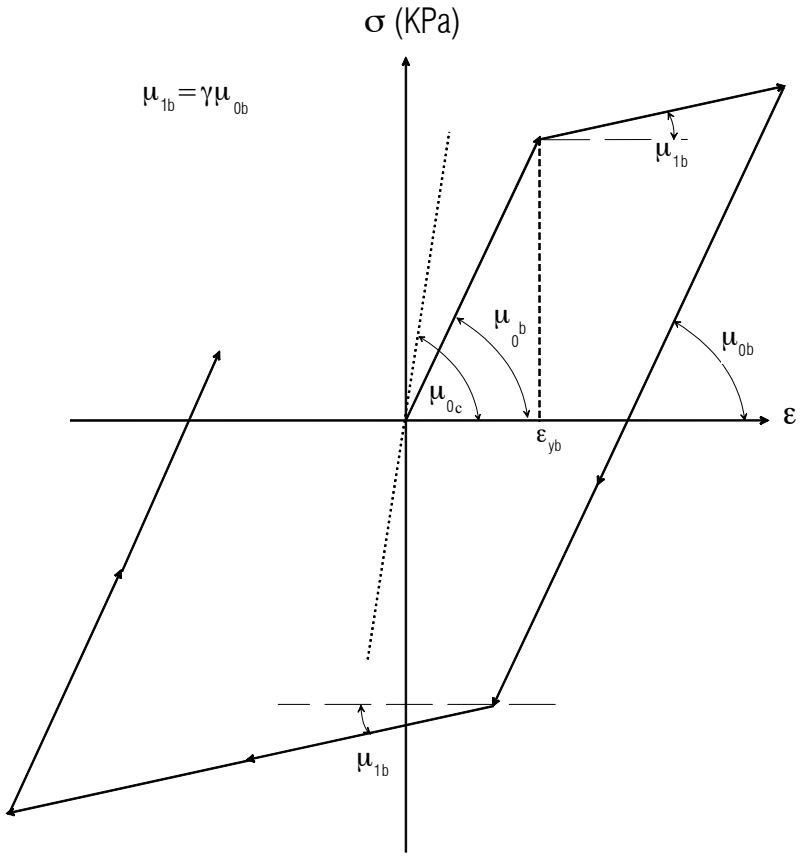

Fig. 8. The constitutive laws, $\sigma - \varepsilon$, for the building (solid line) and for the contacts (dashed line).

The equation of motion is

$$v_t = \frac{1}{\rho}(\sigma)_x \quad , \tag{4.2a}$$

and the relation between the derivatives of the strain and of the velocity is

$$\varepsilon_t = v_x \quad , \tag{4.2b}$$

where v, ρ, σ, and ε are particle velocity, density, shear stress, and shear strain, respectively, and the subscripts t and x represent derivatives with respect to time and space. $v = \frac{\partial u}{\partial t}$ and $\varepsilon = \frac{\partial u}{\partial x}$ are the velocity and the strain of a particle, and u is out-of-plane displacement of a particle along the propagation ray.

Table 4.1 One-dimensional building model

	Inte-rstory Height $h_{interstory}$ (m)	Slab Thickness h_{slab} (m)	$\beta_{inter\text{-}story}$ (m/s)	β_{slab} (m/s)	$\rho_{inter\text{-}story}$ (kg/m3)	ρ_{slab} (kg/m3)
Roof slab		0.203		2000		2384
Seventh story	2.44		73.15		82.90	
Seventh floor slab		0.215		2000		2384
Sixth story	2.44		76.20		82.90	
Sixth floor slab		0.216		2000		2384
Fifth story	2.44		77.72		82.90	
Fifth floor slab		0.216		2000		2384
Fourth story	2.44		79.25		82.90	
Fourth floor slab		0.216		2000		2384
Third story	2.44		91.44		82.90	
Third floor slab		0.216		2000		2384
Second story	2.44		129.50		82.90	
Second floor slab		0.254		2000		2384
First story	3.86		140.20		76.92	

The Lax-Wendroff $O(\Delta t^2, \Delta x^2)$ finite difference method (Gicev 2005, Lax and Wendroff 1964) for a set of simultaneous equations is then used to solve the problem.

The time increment is obtained from the minimum ratio:

$$\Delta t = \left(\frac{\Delta x_1}{\beta_1} \right)_{\min} = \frac{\Delta x_{14}}{\beta_{14}} , \qquad (4.3)$$

where the subscripts stand for the layer numbers counted from the base.

In the numerical model, the building is discretized as follows. The floor layers are discretized with three spatial intervals, while the number of the equal spatial intervals of the interstory layers is $n_l = 3 \cdot h_l / h_{14}$, where subscript stands for the layer number. In this way, we obtain an equidistant grid in the inter-story layers, so that for layer l, for example, the spatial interval is

$$\Delta x_l = \frac{h_l}{n_l} = \frac{h_{14}}{3}. \qquad (4.4a)$$

At the floor levels, the spatial interval is

$$\Delta x_l = \frac{h_l}{3}, \qquad (4.4b)$$

and at the contact points i the spatial interval is

$$\Delta x_i = \frac{\Delta x_{i+1} + \Delta x_{i-1}}{2}, \qquad (4.4c)$$

where i stands for the ordered number of the contact points. The numerical tests have shown that this discretization leads to good and stable results. In this way, the height of the building is discretized by a grid having 295 points and 294 intervals.

Above the top point (N = 295), an additional dummy point N' is introduced, at distance Δx_{14}. For a stress-free point N, for all time, the velocities and the stress at the point N' are updated as

$$v_{N'} = v_{N-1} \qquad (4.5a)$$

$$\sigma_{N'} = -\sigma_{N-1} \quad . \qquad (4.5b)$$

Equations (4.2) can be written in vector form as

$$\frac{\partial \mathbf{U}}{\partial t} = \frac{\partial \mathbf{F}}{\partial x} \quad , \qquad (4.6)$$

where

$$\mathbf{U} = \begin{Bmatrix} v \\ \varepsilon \end{Bmatrix} \quad \text{and} \quad \mathbf{F} = \begin{Bmatrix} \frac{\sigma}{\rho} \\ v \end{Bmatrix} \quad . \qquad (4.7)$$

The vector **U** at point i in time (j+1) Δt expanded in Taylor series is

$$\mathbf{U}_{i,j+1} = \mathbf{U}_{i,j} + \Delta t\left(\frac{\partial \mathbf{U}}{\partial t}\right)_{i,j} + \frac{\Delta t^2}{2}\left(\frac{\partial^2 \mathbf{U}}{\partial t^2}\right)_{i,j} + O(\Delta t^3)\,, \text{ and from Eq.(4.6)}$$

$$\mathbf{U}_{i,j+1} = \mathbf{U}_{i,j} + \Delta t\left(\frac{\partial \mathbf{F}}{\partial x}\right)_{i,j} + \frac{\Delta t^2}{2}\frac{\partial}{\partial t}\left(\frac{\partial \mathbf{F}}{\partial x}\right)_{i,j} + O(\Delta t^3)$$

$$\mathbf{U}_{i,j+1} = \mathbf{U}_{i,j} + \Delta t\left(\frac{\partial \mathbf{F}}{\partial x}\right)_{i,j} + \frac{\Delta t^2}{2}\frac{\partial}{\partial x}\left(\mathbf{A}(\mathbf{U})\frac{\partial \mathbf{F}}{\partial x}\right)_{i,j} + O(\Delta t^3) \quad . \tag{4.8}$$

A(U) is the Jacobian matrix

$$\mathbf{A}(\mathbf{U}) = \frac{\partial \mathbf{F}}{\partial \mathbf{U}} = \begin{bmatrix} \dfrac{\partial \sigma}{\rho \partial v} & \dfrac{\partial \sigma}{\rho \partial \varepsilon} \\ \dfrac{\partial v}{\partial v} & \dfrac{\partial v}{\partial \varepsilon} \end{bmatrix} = \begin{bmatrix} 0 & \dfrac{1}{\rho}\dfrac{d\sigma}{d\varepsilon} \\ 1 & 0 \end{bmatrix} \quad . \tag{4.9}$$

Because the time history of the incident-wave displacements at the base is specified a priori and is assumed to be given by the recorded motion in channel 16 (Fig. 3), and because the top of the building is a stress-free boundary, our problem is a boundary-value problem with mixed boundary conditions, prescribed function (displacement) at the bottom, and prescribed zero derivative (of the displacement) at the top.

Assuming that the stiffness and densities of each floor are known, our goal is to find the best values of the parameters ε_{yb} and γ (Fig. 8) of the bi-linear constitutive law of the 1-D model, so that the computed response agrees with the recorded one.

5. ERROR ANALYSIS

The nature of the problem we are studying is three-dimensional, and its constitutive relations are not bi-linear. Therefore, we cannot expect that the 1-D model will be able to replicate the recorded displacements exactly. With chosen constraints, we use the recorded displacements to find the best values of the parameters $\varepsilon_0 = \varepsilon_{yb}$ and γ, which will be assumed to be same for all soft layers (Fig. 8). The total displacements (linear + non-linear) obtained by our 1-D model versus time are shown in Fig. 9a. The corresponding plastic strain is shown in Fig. 9b. Both plots are presented for the full duration of the record (t = 60 s). It can be seen that the largest response occurs during the first 20 s.

We search for the best values of ε_0 and γ by a trial-and-error procedure in the regions $0.001 \le \varepsilon_0 \le 0.0045$, with increments $\Delta\varepsilon_0 = 0.0005$, and $0.05 \le \gamma \le 0.5$, with increments $\Delta\gamma = 0.05$. For this range, we obtain the model responses for this coarse grid containing the data for 80 different models.

Because the bulk of strong motion energy is concentrated in the first 20 s of the recorded displacements (Fig. 9), in the following we limit our search to those first 20 s only. For each of the mesh points, we obtain the synthetic response $\vec{u}_m(t)$, $0 \le t \le 20$ s at the locations of the recorded responses $\vec{r}_m(t)$, $0 \le t \le 20$ s and then compute the error vectors $\vec{e}_m(t) = \vec{u}_m(t) - \vec{r}_m(t)$. To quantify the four error vectors and to estimate the error, at the second, third, and sixth floors, and at the roof (the respective locations of the recording channels Ch12, Ch11, Ch10, and Ch09), we compute their norm $\mathrm{err}_{2m} = (\vec{e}_m, \vec{e}_m)$. The total error for each point (γ, ε_0) is then chosen to be the sum of the errors in the four specified channels, $\mathrm{err}_2 = \sum_{m=1}^{4} \mathrm{err}_{2m}$. The dependence of $\mathrm{err}_2 = \mathrm{err}_2(\gamma, \varepsilon_0)$ on γ and ε_0 is illustrated in Fig.10a. The minimum of the error for this coarse grid is at (γ, ε_0) = (0.4, 0.0015).

Next, we vary ε_0 and γ in the regions $0.0013 \le \varepsilon_0 \le 0.0022$, with increment $\Delta\varepsilon_0 = 0.0001$, and $0.38 \le \gamma \le 0.47$, with increment $\Delta\gamma = 0.01$. This gives a fine grid with 100 points (γ, ε_0). As for the coarse grid, we obtain the $\mathrm{err}_2 = \mathrm{err}_2(\gamma, \varepsilon_0)$, which is illustrated in Fig. 10b. The minimum of this error appears at (γ, ε_0) = (0.43, 0.0020), and its value is $err_{2\min} = 4.9$.

The results for $\mathrm{err}_{2m}(\gamma, \varepsilon_0)$ at the locations of the recording instruments for the fine grid are presented in Fig. 11. The trend is that for the upper floors (Ch09 and Ch10) the minimum error appears at (γ, ε_0) = (0.43, 0.0020), while for Ch11 the minimum error appears at $\gamma = 0.41$ at smaller ε_0, and at Ch12 at (γ, ε_0) = (0.45, 0.0021). Using the minimum cumulative error, we choose the yielding strain $\varepsilon_0 = 0.002$ and $\gamma = 0.43$ as an approximation for the constitutive law of the material $\sigma = \sigma(\varepsilon)$ in all layers.

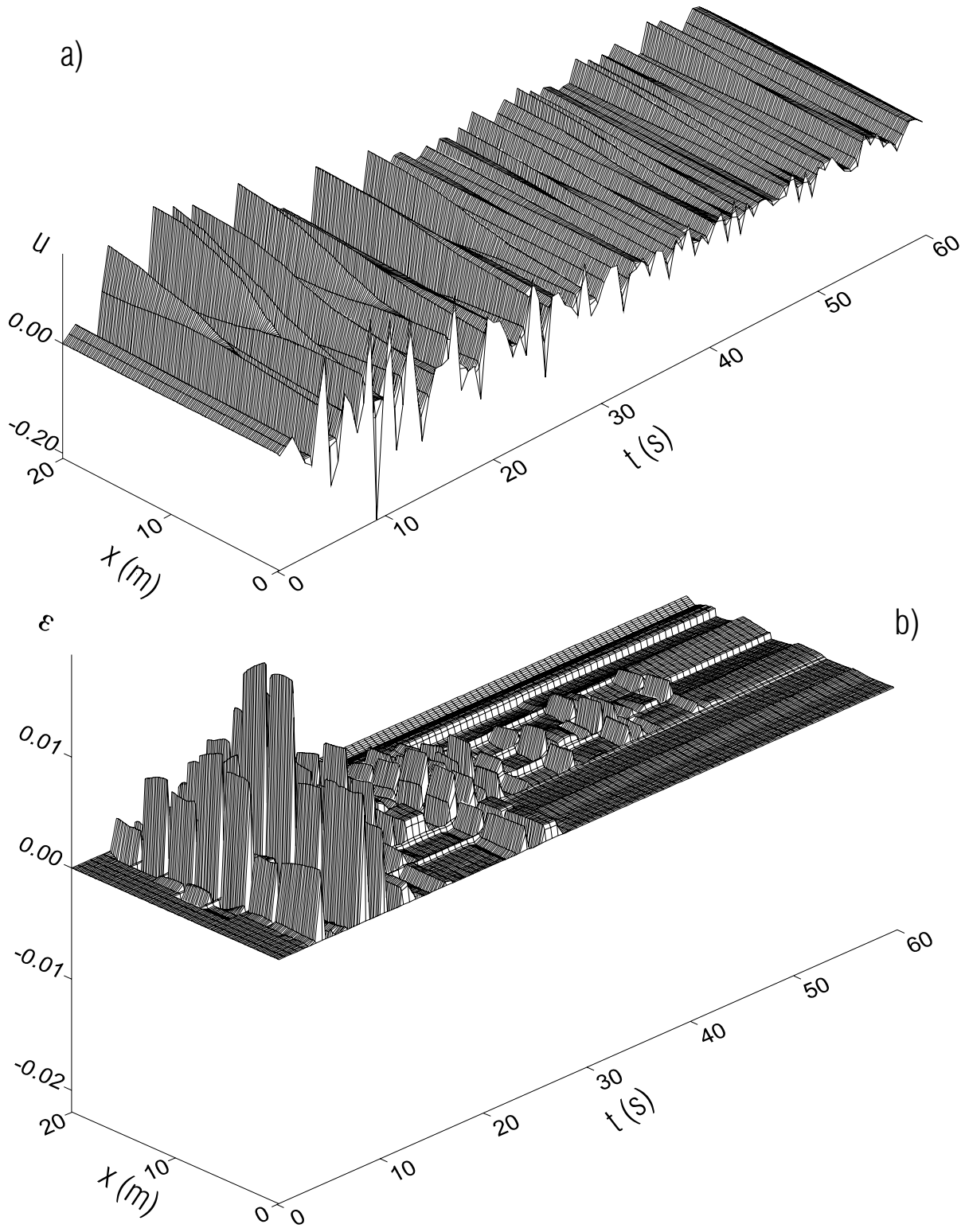

Fig. 9. a) Displacement along the beam (in meters) versus time. b) Permanent strain along the beam versus time.

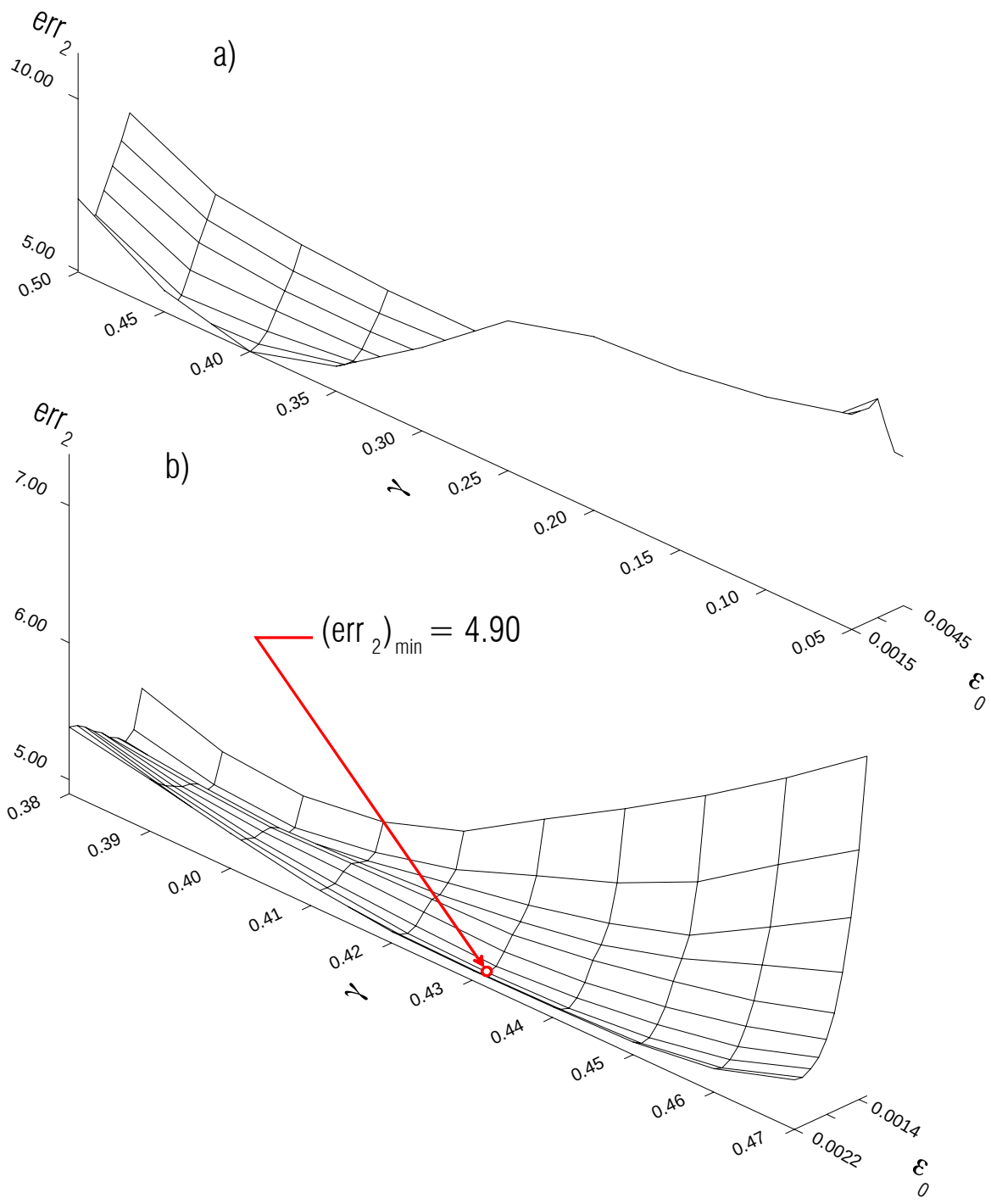

Fig. 10. 2-norm of the cumulative error vector as a function of γ, and the maximum elastic strain, ε_0: a) with coarse grid (γ, ε_0), and b) fine grid (γ, ε_0).

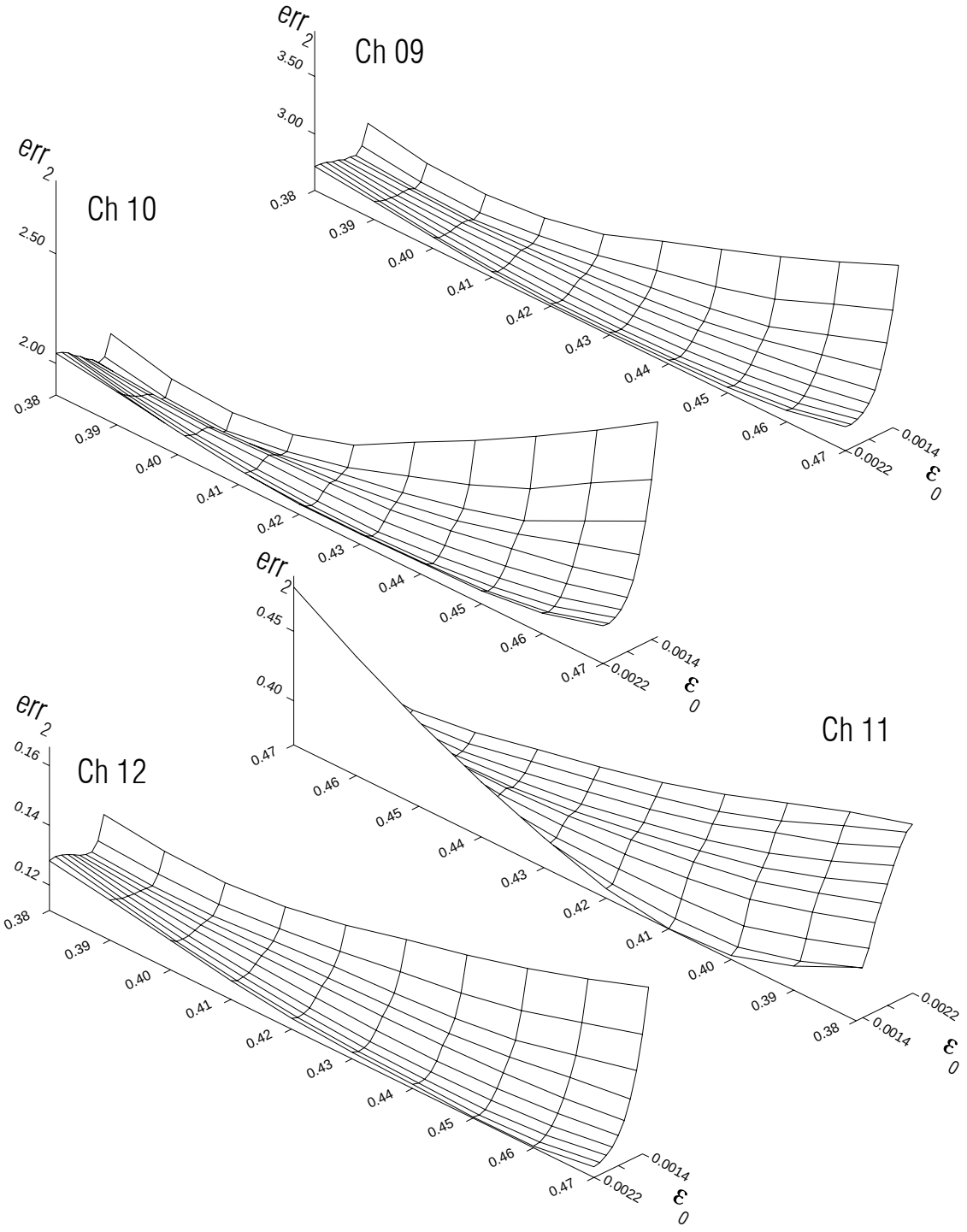

Fig. 11 Errors at the recording channels 9, 10, 11 and 12, versus γ and ε_0.

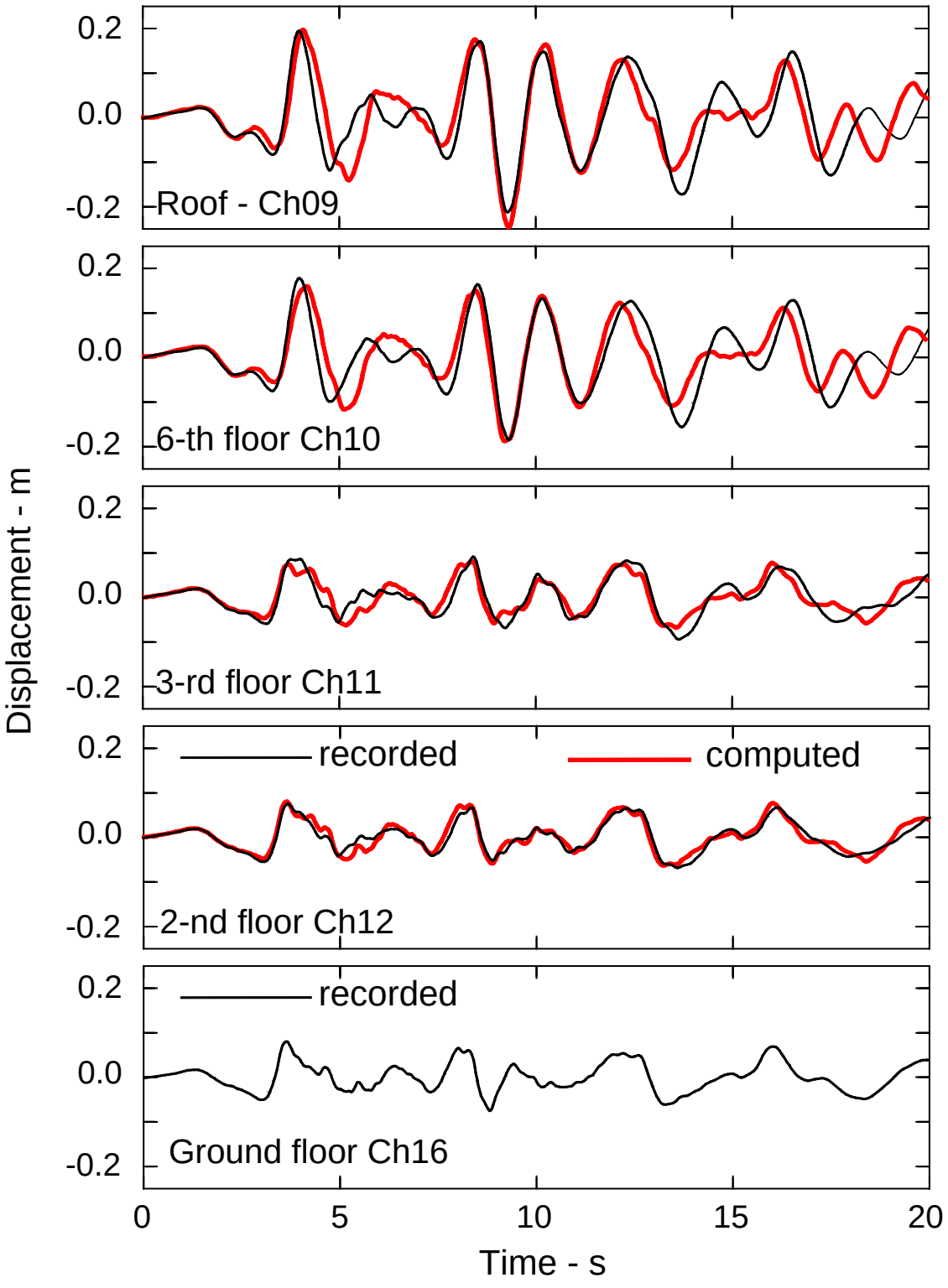

Fig. 12. Comparison of recorded (fine line) and computed (wide line) displacements.

In Fig. 12, the time histories of the recorded (solid line) and computed (wide line) displacements are shown for all recording channels, for $\varepsilon_0 = 0.002$ and $\gamma = 0.43$. We note that the error can be reduced further by varying ε_0 and γ in different layers, and by searching for time dependence of ε_0 and γ. We will present such refinements in our future studies, which will be based on more detailed models.

6. RESULTS

In Fig.13, the field of the total displacements is shown for all beam points. Fig. 14 shows the field of the total displacements at the points where yielding occurred. Both plots describe the first

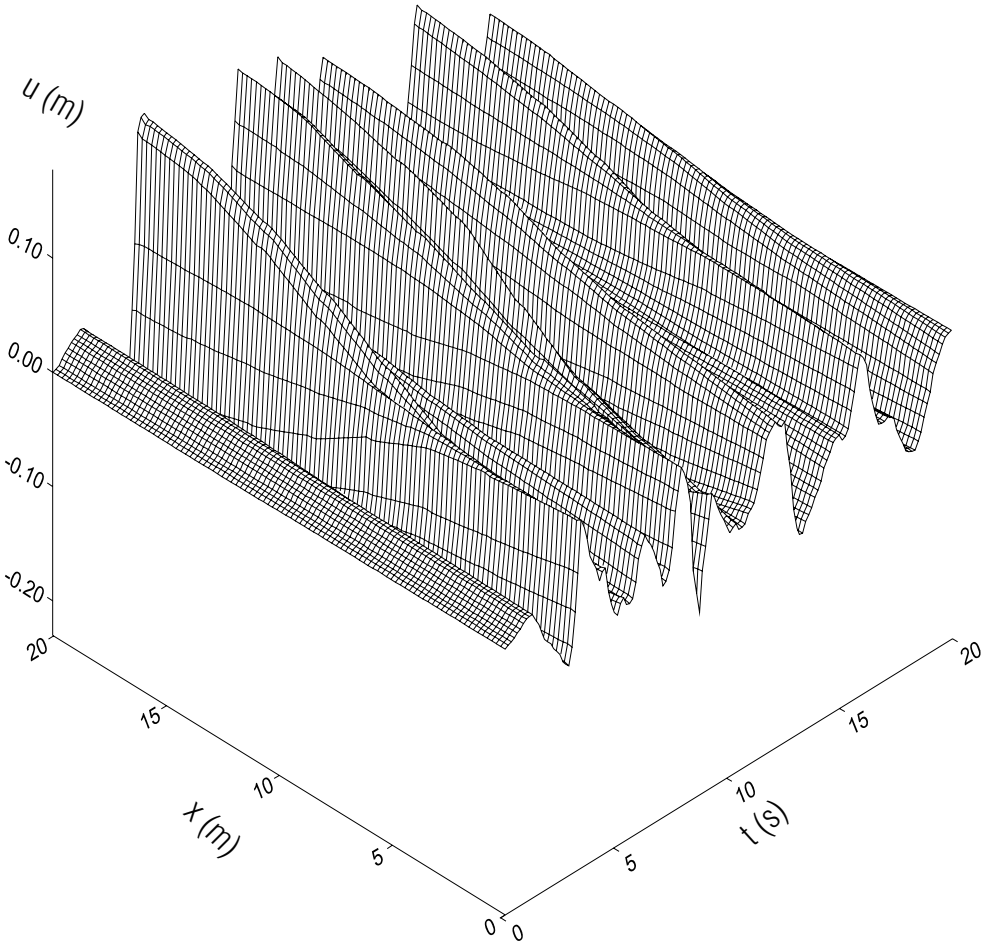

Fig. 13. Total displacement along the beam during the first 20 s of response.

20 s of motion, and it can be seen that up to about t = 4 s the response is linear, while starting at about t = 4 s all the points in the inter-story layers yield. The floor slabs remain linear.

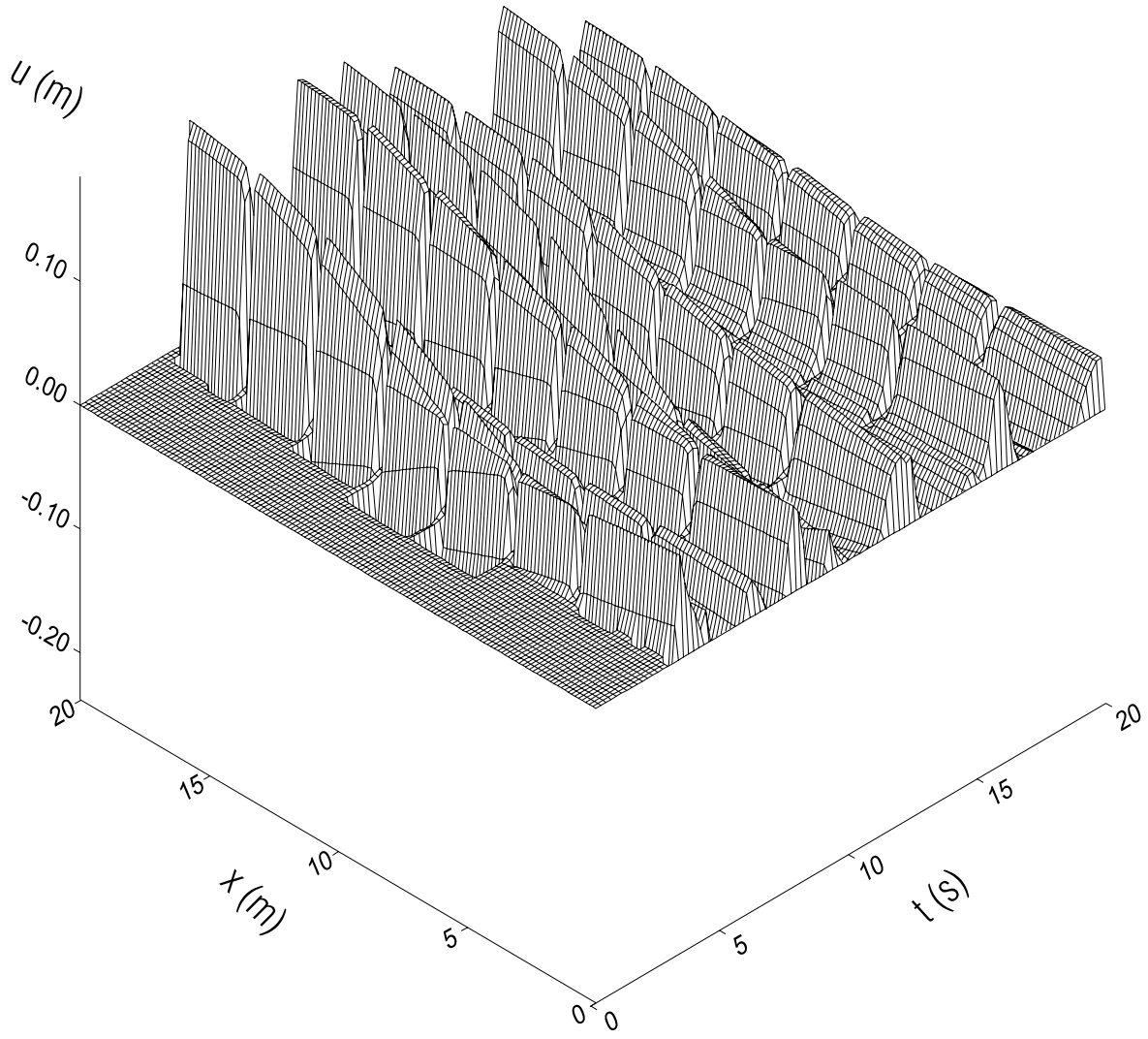

Fig. 14. Displacement along the beam where permanent strain occurred, during the first 20 s of response.

The largest absolute displacement at the top of the building occurs at t = 9.38 s, and the displacement along the beam, u(x) at this instant is shown in Fig. 15a. Also, in this figure, the residual displacement along the beam after the end of the excitation is plotted using a dashed

line. The largest permanent (nonreversible) strains occur in the fourth- and fifth-story columns (seventh and ninth layers), and their values are $\varepsilon_p \approx -0.022$ (Fig. 15b).

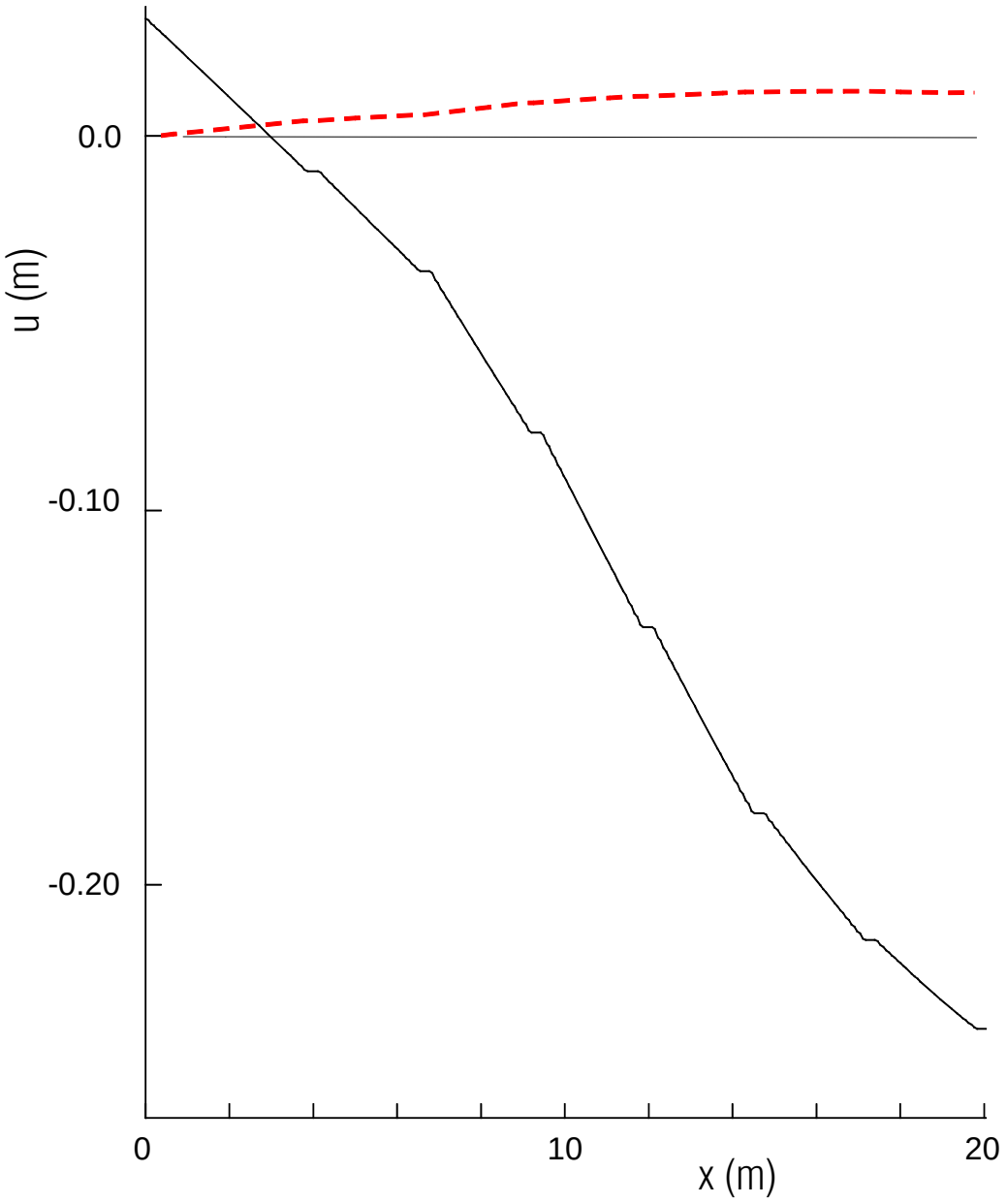

Fig. 15a. Displacement along the the beat at t = 9.38 s when the maximum occurs at the roof (solid line), and 2 s after the end of excitation, at t = 62 s (dashed line).

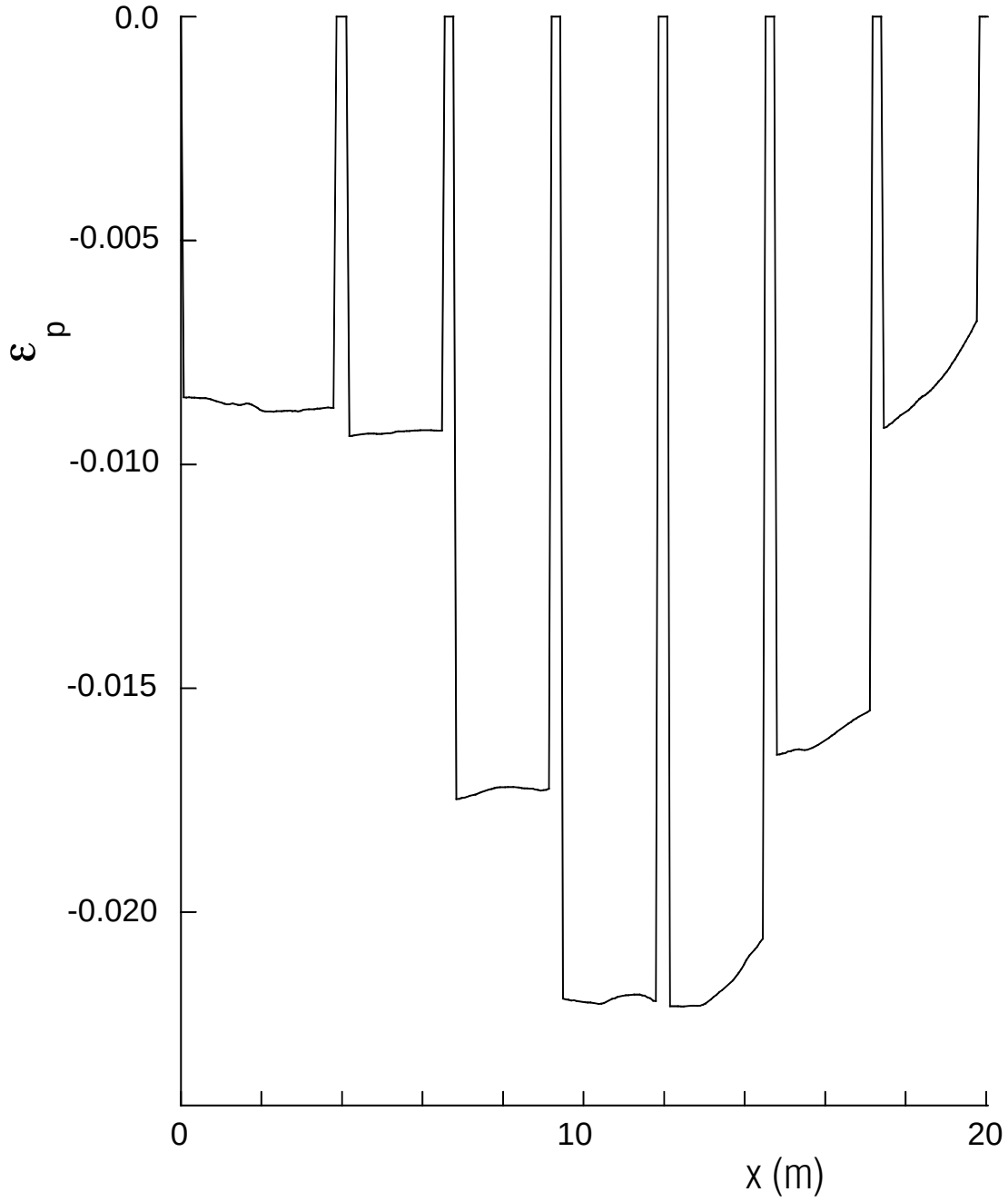

Fig. 15b. Permanent strain along the beam at t =9.38 s, when maximum displacement occurs at the roof.

Fig. 16 shows the permanent strain, ε_{p}, along the beam versus time. Up to approximately 4 s, there is no permanent strain. At about 4 s, all soft layers yield. From 4 to about 8.5 s, the permanent strains are relatively low, and from 8.5 to 10 s permanent strains increase further. After 10 s, the strains in the building are small again (Fig.16).

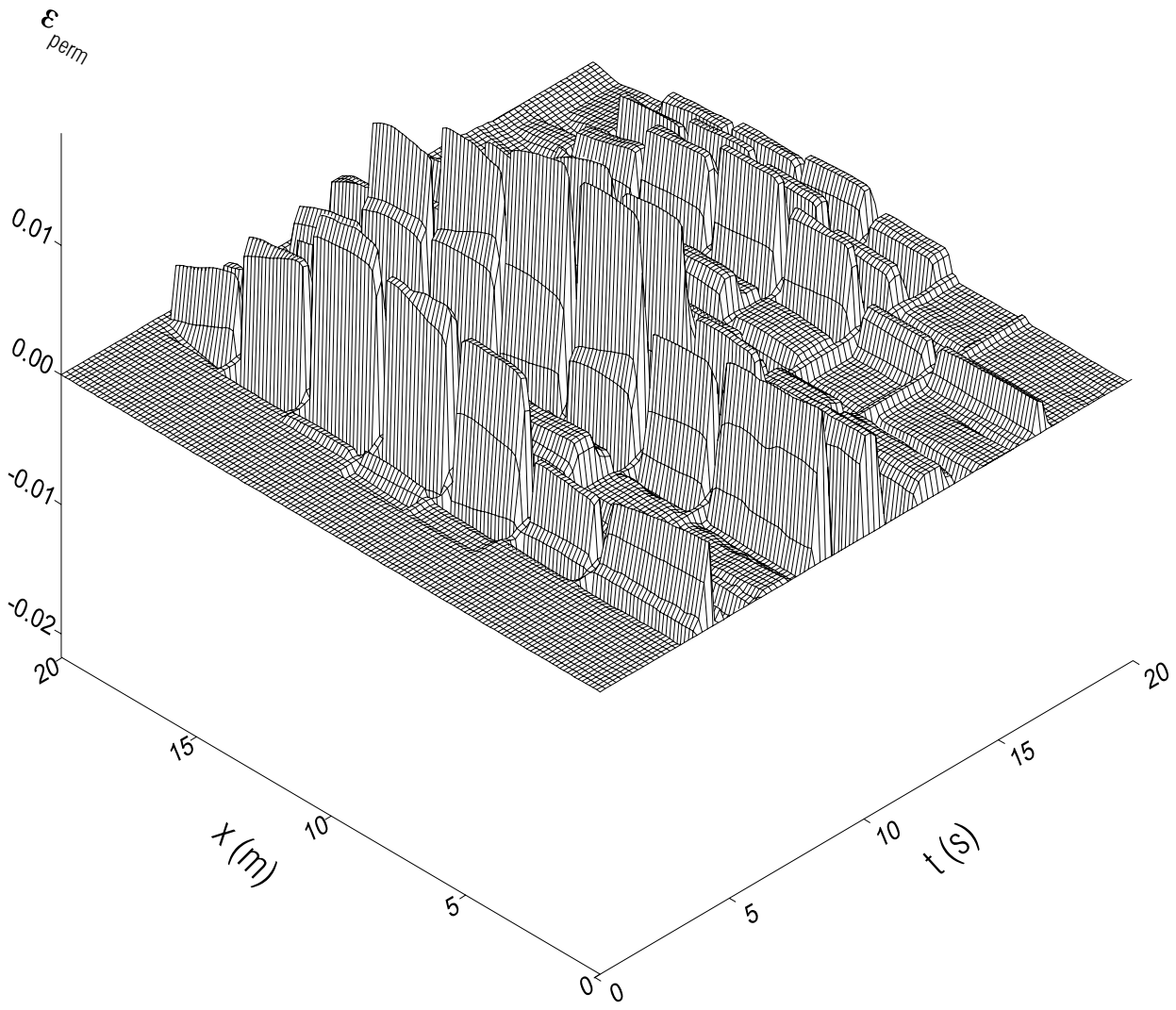

Fig. 16. Permanent strain $\varepsilon_{\mathrm{perm}}$ along the building during the first 20 s of excitation.

Fig. 17 shows the "permanent" ductility, defined as the ratio of the permanent strain and the yielding strain,

$$\mu = \frac{\varepsilon_{\mathrm{p}}}{\varepsilon_{\mathrm{y}}}, \qquad (6.1)$$

as a function of time. This type of plot is useful from the damage detection point of view because it shows when and where the failure in structural members occurred. In Fig. 17a, the positive values, and in Fig. 17b the negative values of permanent ductility are shown.

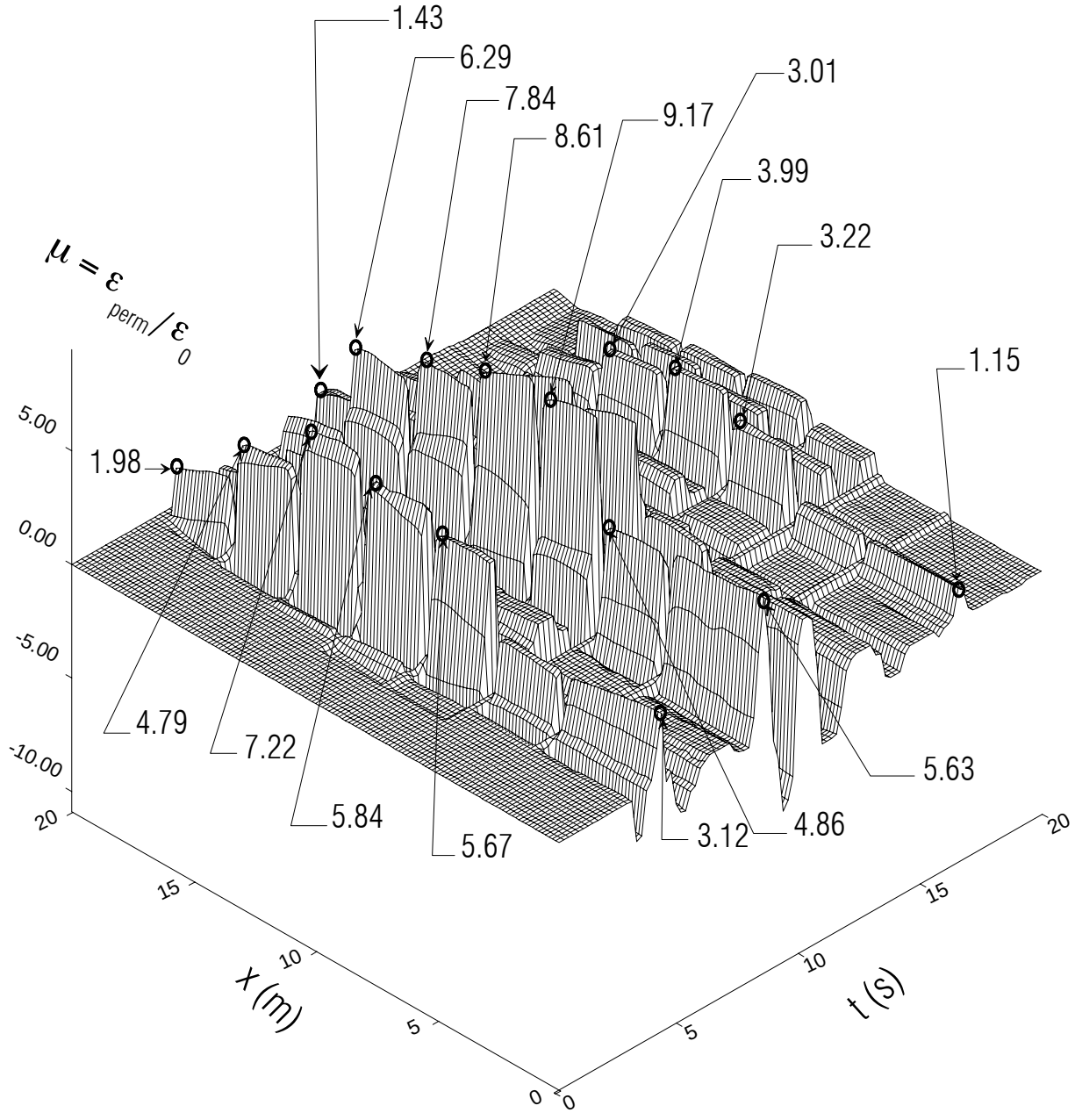

Fig. 17a. The ratio $\mu = \varepsilon_{\text{perm}} / \varepsilon_0$ along the building during the first 20 s of excitation. Positive values.

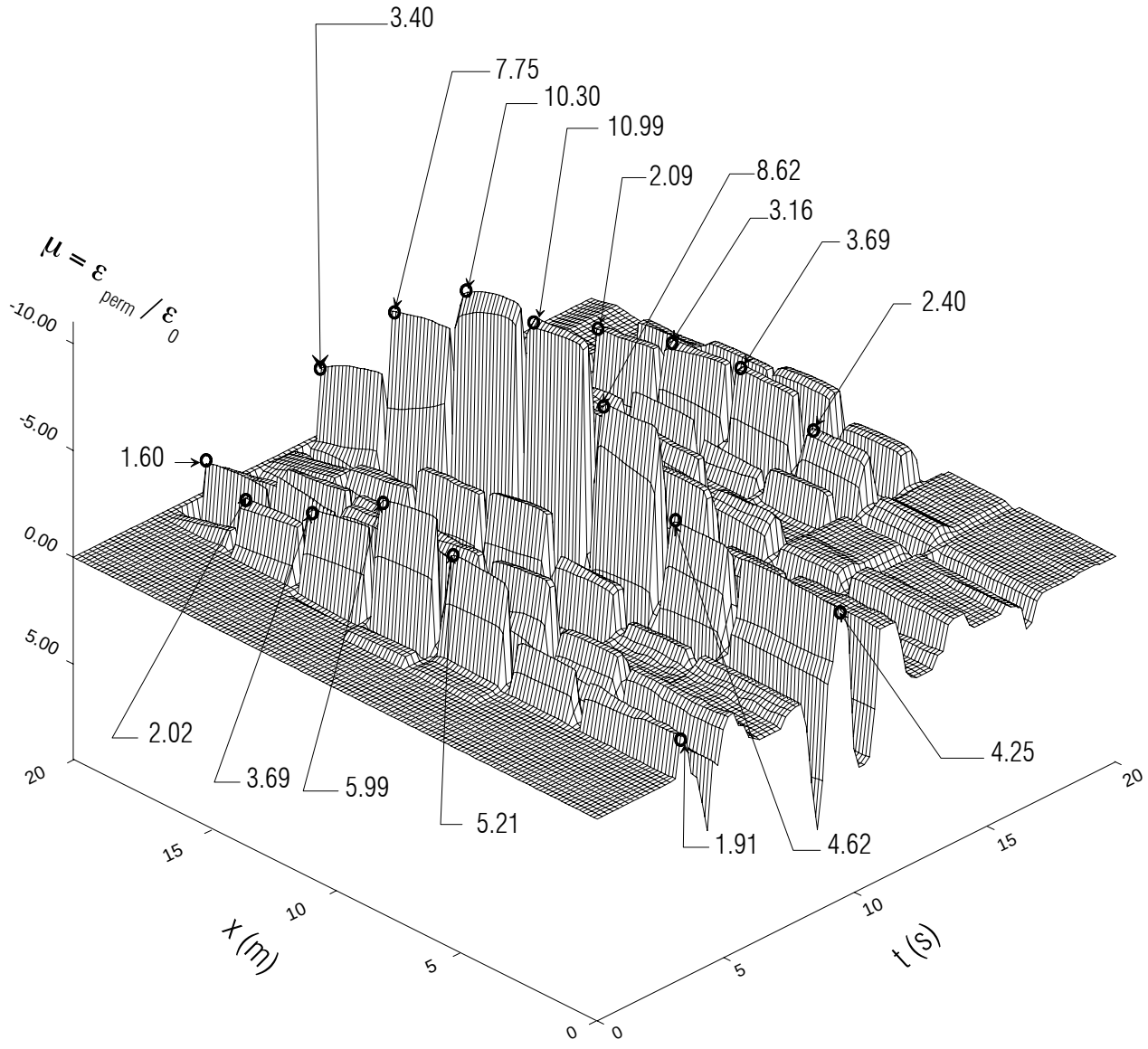

Fig. 17b. The ratio $\mu = \varepsilon_{\text{perm}} / \varepsilon_0$ along the building during the first 20 s of excitation. Negative values.

As can be seen, at t = 9.38 s, when the maxima of the permanent strain occurred, the ductility was the largest and had the value $\mu = -10.99$ in the columns of the fourth floor, just below the spandrel beam, and the fifth floor slab (in the seventh layer of the model, Table 4.1). The ductility in the columns of the fifth floor (ninth layer of the model), was $\mu = -10.30$, close to the largest ductility just below. The maximum of the permanent strain occurred at t = 8.58 s.

Earlier, at t = 4.19 s, at the same location, the ductility reached a positive value of $\mu = 7.22$, while at t = 3.59 s the largest negative ductility, $\mu = -5.99$, occurred in the fourth-story columns

(seventh layer in the model). These were large ductilities, and as we could see after the earthquake, the fourth-story columns were severely damaged, starting at t = 3.59 s and t = 4.19 s and then through t = 9.38 s.

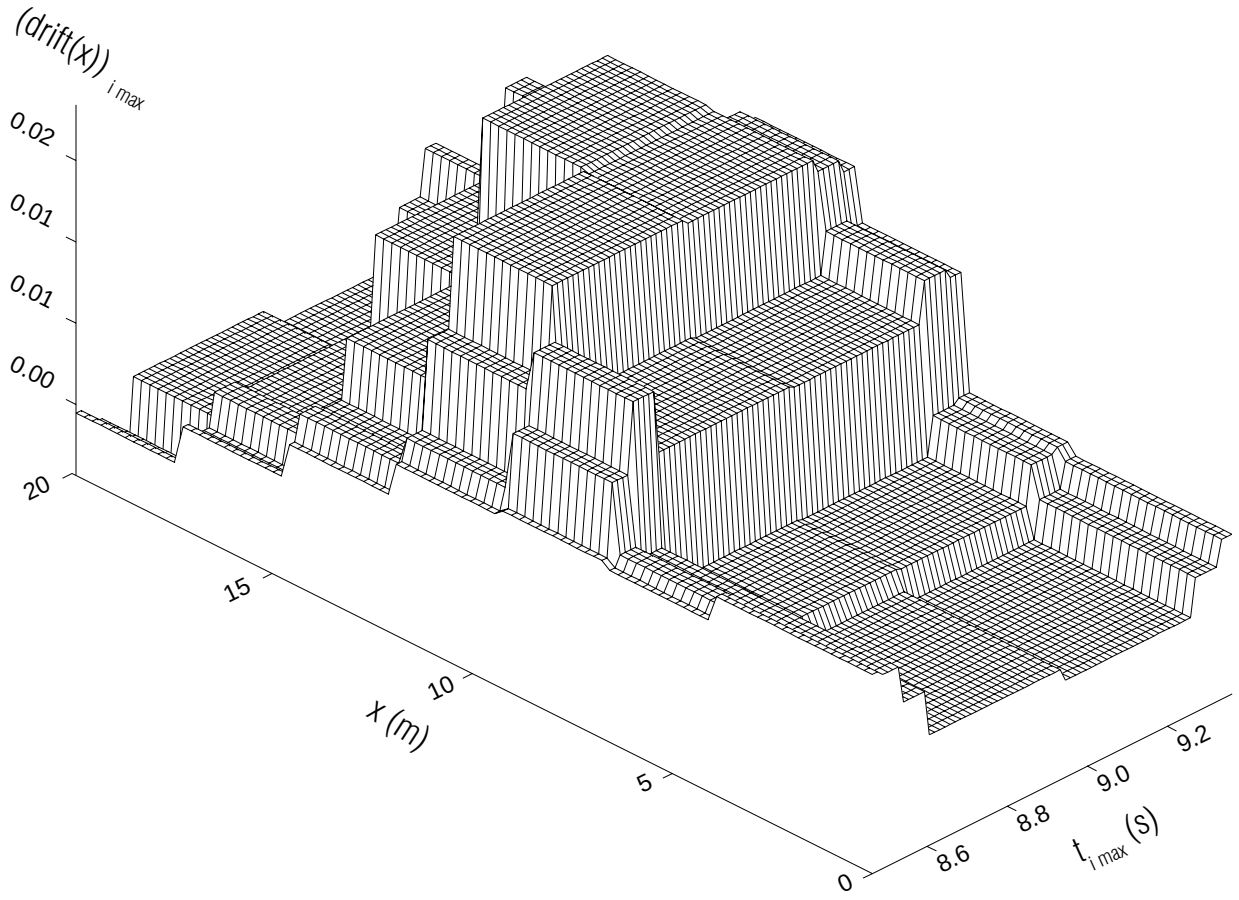

Fig. 18. The interstory drifts along the building, at times when the maxima occur.

Fig. 18 shows the maxima of the drifts along the building height, x(m), where $\text{drift}(l) = \frac{u_{l+1} - u_{l-1}}{h_l}$, and where l stands for the layer number, at the time when those occurred. It can be seen that within about 1 s (from t = 8.5 s to t = 9.5 s) all columns experienced their maximum drifts. In Fig. 19, these drifts are plotted versus the height of the building, and the times when the maxima occurred are shown. The residual drifts, after the shaking stopped, are shown by a dotted line. It can be seen that the largest drifts, equal to 0.023, occurred in the seventh layer (columns of the fourth story) at time t_4 = 8.64 s.

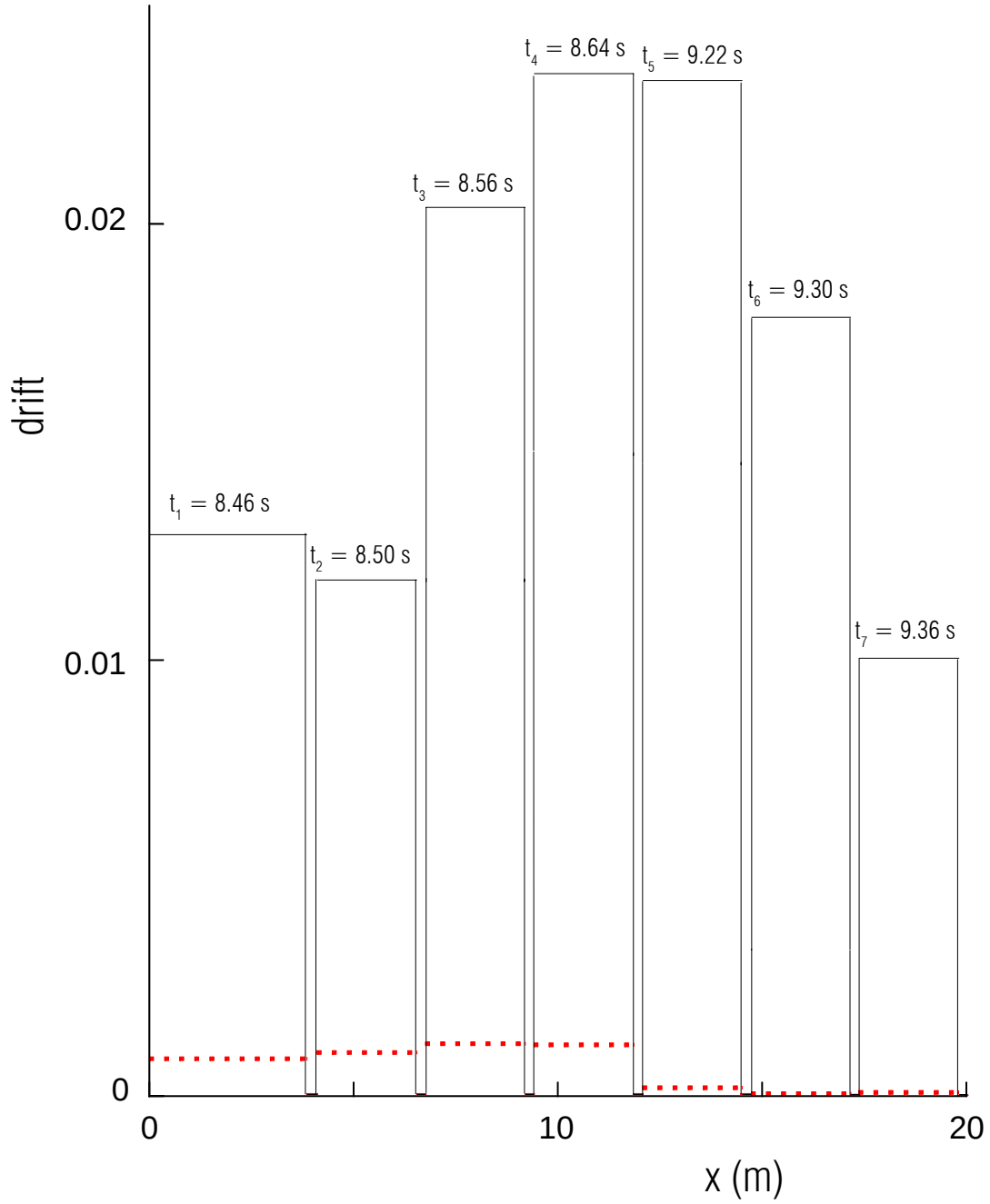

Fig. 19. Maxima of the interstory drifts in the Holiday Inn building during Northridge earthquake, showing time when those occur (solid line), and at two seconds after the end of excitation, at t = 62 s (dashed line).

Figures 18 and 19 show that the peak inter-story drifts propagated up, apparently as a strong-motion pulse entered and propagated up the building with velocity of about 55 m/s, reaching the maximum values between 8.46 s and 8.84 s. The largest drift occurred between the fourth and fifth floors, precisely at the location where the damage could be seen after the earthquake (Fig.

4). Upon reflection from the roof, the displacements (and drift) amplitudes doubled, as this burst of strong-motion energy continued on its path downward. This doubling of the amplitudes in turn increased the drifts at the fifth, sixth, and seventh floors (Figs. 18 and 19). As this down-propagating energy encountered the broken columns (just below the fifth floor slab) it lost enough energy, and in its propagation down it did not further increase the peak drifts at the fifth through first floors, which were created during the preceding 0.2 to 0.3 s.

The above apparent velocity of 55 m/s, associated with upward propagation of peak strain, is in agreement with the average speed of shear waves, 54.8 m/s, during the time window of $7 < t < 12$ s (Todorovska and Trifunac 2006d), estimated via impulse-response travel-time analysis. This shows that the occurrence of peak strains is associated with propagation of prominent ground motion pulses and the waves those pulses produce in the buildings. It shows that the peak drifts can occur during one travel time, up or down the building, or during one quarter of the fundamental, fixed-base period of the building, $T_1/4$. Neither the vertical distribution of the peak drift amplitudes, nor the time of their occurrence, can be described directly by the Response Spectrum Method of analysis.

In engineering design, the drifts can be used to calculate the inter-story forces. Assuming fixed-fixed column ends, these forces are

$$\frac{12EI}{h_l^3}\left(u_{l+1} - u_{l-1}\right) = F_l \ , \qquad (6.2a)$$

or, using the drift,

$$\frac{12EI}{h_l^3} \cdot \text{drift} = \frac{F_l}{h_l} . \qquad (6.2b)$$

In the above equations, E is the modulus of elasticity, I is the moment of inertia of the column cross section, u is displacement of the "rigid" floor, h is the height of the column, and F is the inter-story force. The subscript l stands for the order number of the column. Having E and I, all of the inter-story forces can be evaluated, and the equivalent static analysis of the building can be performed.

Summarizing the above results, the maximum ductilities (Fig.17a,b) and the maximum inter-story drifts (Fig.19), as well as the ratios between the maximum strains $\varepsilon_{max} = \varepsilon_y + \varepsilon_p = \left(1 + \mu_{max}\right) \cdot \varepsilon_y$ (see the definition of the permanent ductility in Eq. 6.1) and the maximum inter-story drifts at different layers are as shown in Table 6.1.

Table 6.1

Layer i	$\lvert\mu\rvert_{max}$ (permanent ductility Fig. 17a,b)	$\lvert drift\rvert_{max}$	$\frac{(1+\lvert\mu\rvert_{max})\cdot\varepsilon_{yi}}{\lvert drift\rvert_{max}}$
1	4.25	0.01286	0.817
2	4.86	0.01182	0.991
3	8.62	0.02036	0.999
4	10.99	0.02343	1.023
5	10.30	0.02327	0.971
6	7.75	0.01784	0.981
7	3.90	0.01003	0.877

As would be expected, it can be seen from the last column in this table that the maximum strains are approximately equal to the maximum drifts.

7. PUSH-OVER ANALYSIS

For the static push-over analysis, we use the properties of the building (Table 4.1) represented by one-dimensional shear-beam model. For the wave-propagation analysis, the boundary condition at the bottom was the prescribed displacement. For the static analysis, there is zero displacement at this boundary. At the top of the beam, we use the same boundary condition as that used for the wave propagation analysis—zero derivative of the displacement with respect to the vertical coordinate.

We describe the static load as follows. We define $f(H_b) = f_0$, and $f(0) = 0$, where $f(x)$ is the horizontal force per unit volume. For $F = fr \cdot W_b$, where F is horizontal force per unit square (width = 1, length = 1) of the building, fr is the fraction 0 < fr < 1, and $W_b = \sum_{i=1}^{14} \rho_i h_i$ is the weight of the building per unit square (width = 1, length = 1), we have $\frac{f_0 \cdot H_b}{2} = F$ and $f_0 = \frac{2F}{H_b}$.

From equilibrium at an arbitrary point x and for triangular distribution of static load

$$\left(\sigma + \frac{\partial \sigma}{\partial x} dx - \sigma\right) dy \cdot dz = -f(x) \cdot dx \cdot dy \cdot dz \qquad (7.1)$$

or

$$\frac{\partial \sigma}{\partial x} = -f(x) \quad , \tag{7.2}$$

where $f(x) = \frac{f_0 \cdot x}{H_b}$,

and for a cell i $\left(x \in \left[x_i - \frac{\Delta x_i}{2}, x_i + \frac{\Delta x_i}{2} \right] \right)$, approximating (7.2) by Finite Differences (FD):

$$\frac{\sigma_{i+1/2} - \sigma_{i-1/2}}{\Delta x} = -f(x_i). \tag{7.3}$$

Assuming linear stress and approximating (7.3), we have:

$$\frac{\mu_{i+1/2} \frac{u_{i+1} - u_i}{\Delta x_{i+1}} - \mu_{i-1/2} \frac{u_i - u_{i-1}}{\Delta x_{i-1}}}{\Delta x_i} = -\frac{f_0 \cdot x_i}{H_b} \quad . \tag{7.4}$$

By solving the system $\mathbf{Au} = \mathbf{F}$, where $\mathbf{A}$ is the tri-diagonal (n - 1,n - 1) matrix

$$A = \begin{bmatrix} -\frac{\mu_{2,3}}{\Delta x_3 \Delta x_2} & -\frac{\mu_{2,1}}{\Delta x_1 \Delta x_2} & \frac{\mu_{2,3}}{\Delta x_3 \Delta x_2} & 0 & . & . & . & . & . & 0 \\ . & & & & & & & & & . \\ 0 & & . & 0 & \frac{\mu_{1,i-1}}{\Delta x_{i-1} \Delta x_i} & -\frac{\mu_{1,i+1}}{\Delta x_{i+1} \Delta x_i} - \frac{\mu_{1,i-1}}{\Delta x_{i-1} \Delta x_i} & \frac{\mu_{1,i+1}}{\Delta x_{i+1} \Delta x_i} & 0 & . & 0 \\ . & & & & & & & & & . \\ . & & & & & & & & & . \\ . & & & & & & & & & . \\ . & & & & & & & & & . \\ . & & & & & & & & & . \\ 0 & & . & . & . & . & 0 & 0 & \frac{2\mu_N}{\Delta x_N^2} & -\frac{2\mu_N}{\Delta x_N^2} \end{bmatrix}$$

and

$$F = \frac{f_0}{H_b}\begin{Bmatrix} x_2 \\ x_3 \\ . \\ . \\ . \\ . \\ . \\ . \\ x_N \end{Bmatrix}$$ is the load vector,

we can find the displacement vector

$$u = \begin{Bmatrix} u_2 \\ u_3 \\ . \\ . \\ . \\ . \\ . \\ . \\ u_N \end{Bmatrix} \quad \text{and } u_1 = 0 . \tag{7.5}$$

This is the linear solution. The next step is to compare the strains $\varepsilon_{1,2} = \frac{u_2 - 0}{x_2 - x_1}$; $\varepsilon_{2,3} = \frac{u_3 - u_2}{x_3 - x_2}; \ldots; \varepsilon_{i,i+1} = \frac{u_{i+1} - u_i}{x_{i+1} - x_i}; \ldots; \varepsilon_{N-1,N} = \frac{u_N - u_{N-1}}{x_N - x_{N-1}}$ with the yielding strain $\varepsilon_y = 0.002$ (see the description of the trial-and-error procedure in section 5, which gives the best values for $(\gamma, \varepsilon_y) = (0.43, 0.002)$.

If $\varepsilon_{i,i+1} > \varepsilon_y$, the displacements in Eq. (7.5) should be recalculated by rearranging the coefficients of the matrix A (which are related to the displacements u_i and u_{i+1}) by adding a term in the vector F at the location of f_i and f_{i+1}, as in the following.

The non-linear static stress between the points i and i+1 for the bi-linear constitutive law can be expressed as

$$\sigma_{i,i+1} = \mu_{i+1/2}\left(\varepsilon_y + \gamma\varepsilon_p\right), \qquad (7.6)$$

where in our example $\varepsilon_y = 0.002$ is the yielding strain that is assumed to be the same everywhere in the building.

Because $\varepsilon_p = \varepsilon - \varepsilon_y = \dfrac{u_{i+1} - u_i}{x_{i+1} - x_i} - \varepsilon_y$, the equation (7.6) can be rewritten as

$\sigma_{i,i+1} = \mu_{i+1/2} \cdot \gamma \cdot \dfrac{u_{i+1} - u_i}{\Delta x_{i+1}} + \mu_{i+1/2}(1-\gamma)\varepsilon_y$, which means that the system of equations corresponding to the i^{th} and $(i+1)^{st}$ term will be modified as

$$\begin{bmatrix} & 0 & . & . & . & . & 0 \\ . & & & & & & . \\ 0 \;.\; 0 & \dfrac{\mu_{i,i-1}}{\Delta x_{i-1}\Delta x_i} & -\dfrac{\gamma\mu_{i,i+1}}{\Delta x_{i+1}\Delta x_i} - \dfrac{\mu_{i,i-1}}{\Delta x_{i-1}\Delta x_i} & \dfrac{\gamma\mu_{i,i+1}}{\Delta x_{i+1}\Delta x_i} & 0 & . & 0 \\ . & & \dfrac{\gamma\mu_{i+1,1}}{\Delta x_{i+1}\Delta x_i} & -\dfrac{\mu_{i+2}}{\Delta x_{i+2}\Delta x_{i+1}} - \dfrac{\gamma\mu_{i+1}}{\Delta x_{i+1}\Delta x_i} & \dfrac{\mu_{i+2}}{\Delta x_{i+2}\Delta x_{i+1}} & & . \\ . & & & & & & . \\ . & & & & & & . \\ . & & & & & & . \\ . & & & & & & . \\ 0 \;.\; . & . & . & 0 & 0 & & \end{bmatrix} \cdot \begin{Bmatrix} u_2 \\ . \\ u_i \\ u_{i+1} \\ . \\ . \\ . \\ . \\ u_N \end{Bmatrix} =$$

$$= -\frac{f_0}{H_b} \begin{Bmatrix} . \\ . \\ x_i \\ x_{i+1} \\ . \\ . \\ . \\ . \\ . \end{Bmatrix} - \begin{Bmatrix} . \\ . \\ \mu_{i,i+1}(1-\gamma)\varepsilon_y \\ -\mu_{i,i+1}(1-\gamma)\varepsilon_y \\ . \\ . \\ . \\ . \\ . \end{Bmatrix} . \qquad (7.7)$$

Solving Eq. (7.7), we obtain the corrected static solution for triangular load vector.

The pair (displacement u_N, fraction fr) then gives one point on the push-over curve for the triangular load.

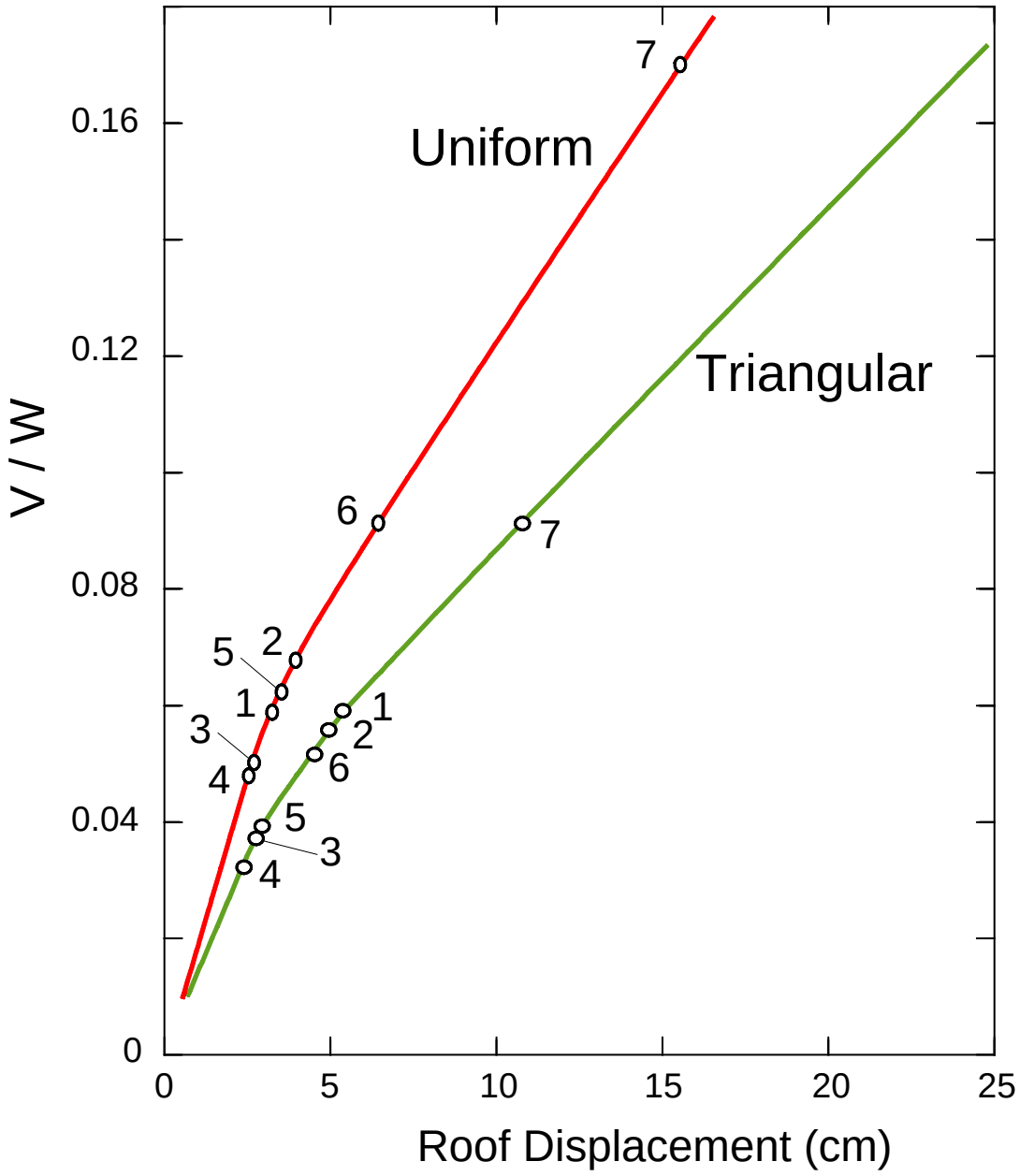

Fig. 20. Push-over curves for one-dimensional model described in Table 4.1 and for triangular and uniform load distributions.

For uniform load vector, the system of equations is the same, except that for the load vector, all of the components become the same and equal to $f = \frac{W_b}{H_b}$.

The computed push-over curves for horizontal uniform load $f_0 = \frac{V}{H_b}$ and for triangular load $f_0 = \frac{2V}{H_b}$ are shown in Fig. 20. The coordinates of the first yield points (circles in Fig. 20) in different inter-story layers are shown in Table 7.1 (for uniform load) and Table 7.2 (for triangular load) sorted by the amplitude of V / W.

Table 7.1 Occurrence of yield points in different layers for uniform load

Inter-story layer i	V/W	u_{roof} (cm)
4	0.052	2.61
3	0.053	2.67
1	0.061	4.02
5	0.066	4.46
2	0.071	5.34
6	0.095	9.27
7	0.174	18.08

As can be seen from the tables, the first yielding occurs in the fourth-story columns for approximately the same roof displacement and for both the triangular and uniform load cases. The yielding then occurs next at the third story.

Table 7.2 Occurrence of yield points in different layers for triangular load

Inter-story layer i	V/W	u_{roof} (cm)
4	0.037	2.62
3	0.040	3.21
5	0.041	3.76
6	0.055	7.09
2	0.059	7.55
1	0.062	9.23
7	0.094	11.99

The yielding at the bottom (the first story) occurs for the same horizontal shear force, and the top column yields last in both load cases. After the yielding in the columns of the fourth and third stories has occurred, for triangular load the upper stories (five and six) yield earlier than the lower stories (two and one), while for the uniform load the lower stories yield earlier than the upper stories (floor one yields earlier than five, and two yields earlier than six).

8. CONCLUSIONS

Using the simple one-dimensional finite-difference representation of a non-linear model, we showed that it is possible to interpret details of the response of a real seven-story hotel building in Van Nuys, California, which was excited by strong ground motion during the 1994 Northridge earthquake. The characteristic damage to this building occurred in the fourth-story columns, just below the spandrel beam along the fifth-story slab during the time interval between 4 and 9 s from the beginning of the shaking. With our simple model, we were able to confirm these observations and to show why this failure occurred at this location.

This study shows that the finite difference calculations can be used successfully even for the simplest representation of a building and with non-linear wave propagation through an equivalent continuous model. This also shows that even with a simple wave-propagation approach one can predict the response characteristics that are obviously present in buildings during earthquakes but that cannot be deciphered by a response analysis based on the concept of the response spectrum (Biot 1932; 1934; 1941; 1942) or by push-over analysis, which favors that part of the response that is close to the first linear mode shape.

The static push-over analysis of the layered shear-beam model of the VN7SH building predicts the first occurrence of non-linear response at the fourth and third floors, which is followed by the initiation of the non-linear response at the first, fifth, second, sixth, and finally the seventh floors, for the assumed uniform load distribution (and similarly at the fourth, third, fifth, sixth, second, first, and seventh floors for the triangular load), for the roof displacements between 2.6 cm and 18.1 cm. Our wave propagation analysis shows, however, that the occurrence of non-linear drifts is governed by the passage of large strong-motion pulses that propagate up and down the building during time intervals that are on the order of $T_1/4$, where T_1 is the period of the fixed-base model of the building, in its current linear or non-linear state of response. In VN7SH, during the 1994 Northridge earthquake, T_1 increased from about 1.1 s, during the first 3 s of response, to 1.5 s, from 25 < t < 60 s of shaking. During the time window from 7 to 12 s, when the largest response and most severe damage occurred, the average value of T_1 was 1.47 s, and $T_1/4$ was about 0.37 s (Todorovska and Trifunac 2006d).

Fig. 5 shows that in terms of the push-over analysis, the stiffness of our FD model of VN7SH is in excellent agreement with all previous studies for relative roof displacements up to about 6 in. Beyond this amplitude, our model continues to deform with constant slope, determined by $\gamma =$ 0.43 and the triangular or uniform distribution load, while the discrete models lead to the column failures and to formation of mechanisms. The agreement of these approaches is to be expected, because all previous studies as well as the present study must satisfy the observed period of vibration during the recorded earthquake response. The principal differences between the present and the previous studies are the consequence of the continuous (this study) versus discrete (all previous studies) representations of the building model. The continuous FD model can represent realistically short waves in the building, which makes it possible to consider, and to analyze, the consequences of abrupt high-frequency pulses associated with near-field ground motion, resulting in linear and non-linear response. The discrete models, with lumped mass at the floor levels, present a low-pass filtered view of the short strong-motion pulses, and thus cannot describe accurately for time and space evolution of the non-linear response.

Strong ground motion can be viewed as a sequence of pulses that propagate up and down the building, reflect off the roof, and create zones of non-linear response, which depend upon the amplitudes and the duration of those pulses. Such representations not only broaden our understanding of the true nature of the non-linear response but also allow us to predict and then to control certain unwanted features of non-linear response that are associated with strain localization, interference, and amplification of non-linear deformations.

The application of the method we employed in this paper is not limited to equivalent, homogeneous, layered representation of the building. We chose such a simple model only to illustrate the method and to test its potential for excitation with relatively long incident seismic waves. Geometrically far more detailed finite-difference models, in two and three dimensions, can easily be constructed and implemented.

REFERENCES

1. Biot, M.A. (1932). Vibrations of Buildings During Earthquakes, Chapter II in Ph.D. Thesis No. 259, entitled *Transient Oscillations in Elastic Systems*, Aeronautics Department, Calif. Inst. of Tech., Pasadena, California.
2. Biot, M.A. (1934). Theory of vibration of buildings during earthquakes," *Zeitschrift für. Angewandte Matematik und Mechanik*, *14*(4), 213–223.
3. Biot, M.A. (1941). A mechanical analyzer for the prediction of earthquake stresses, *Bull. Seism. Soc. Amer*., 31, 151–171.

4. Biot, M.A. (1942). Analytical and experimental methods in engineering seismology, *ASCE Transactions*, 108, 365–408.

5. Blume, J.A., and Assoc. (1973). Holiday Inn, Chapter 29 *in San Fernando, California Earthquake of February 9, 1971,* Volume I, Part A, U.S. Dept. of Commerce, National Oceanic and Atmospheric Administration, Washington, D.C.

6. Browning, J.A., Li, R.Y., Lynn, A., and Moehle, J.P. (2000). Performance assessment for a reinforced concrete frame building. *Earthquake Spectra*, *16*(3), 541–555.

7. De la Llera, J.C., Chopra, A.K., and Almazan, J.L. (2001). Three-dimensional inelastic response of an RC building during the Northridge earthquake. *J. of Structural Eng., ASCE*, *127*(5), 482–489.

8. Gicev, V. (2005). Investigation of Soil-Flexible Foundation-Structure Interaction for Incident Plane SH Waves, Ph.D. Dissertation, Dept. of Civil Engineering, Univ. Southern California, Los Angeles, California.

9. Gicev, V., and Trifunac, M.D. (2006). Permanent deformations and strains in a shear building excited by a strong motion pulse, *Soil Dynamics and Earthquake Engineering,* **26**(12), 1149-1160.

10. Islam, M.S. (1996). Analysis of the response of an instrumented 7-story non-ductile concrete frame building damaged during the Northridge earthquake. Professional Paper 96-9, Los Angeles Tall Building Structural Design Council, 1996 Annual Meeting.

11. Ivanović, S., Trifunac, M.D., Novikova, E.I., Gladkov, A.A., and Todorovska, M.I. (1999a). Instrumented 7-Story Reinforced Concrete Building in Van Nuys, California: Ambient Vibration Survey Following the Damage from the 1994 Northridge earthquake, Dept. of Civil Eng., Rep. No. CE 99-03, Univ. of Southern California, Los Angeles, California.

12. Ivanović, S., Trifunac, M.D., and Todorovska, M.I. (1999b). On identification of damage in structures via wave travel times. *Proc. NATO Workshop on Strong Motion Instrumentation for Civil Engineering Structures,* June 2–5, Istanbul, Turkey, Kluwer Academic Pub., Dordrecht , (2001), 447–468.

13. Ivanović, S., Trifunac, M.D., Novikova, E.I., Gladkov, A.A., and Todorovska, M.I. (2000). Ambient vibration tests of a seven story reinforced concrete building in Van Nuys, California, damaged by the 1994 Northridge earthquake, *Soil Dynamics and Earthquake Eng., 19*(6), 391–411.

14. Kanai, K. (1965). Some new problems of seismic vibrations of a structure, *Proc. Third World Conf. on Earthquake Engineering*, Auckland and Wellington, New Zealand, January 22–February 1, 1965, pp. II-260 to II-275.

15. Lax, P.D., and Wendroff, B. (1964). Difference Schemes for Hyperbolic Equations with High Order of Accuracy, *Comm. on Pure and Applied Mathematics,* **XVII**, 381–398.

16. Li, Y.R., and Jirsa, J.O. (1998). Nonlinear analyses of an instrumented structure damaged in the 1994 Northridge earthquake, *Earthquake Spectra*, *14*(2), 265–283.

17. Loh, S-H., and Lin, H-M. (1996). Application of off-line and on-line identification techniques to building seismic response data, *Earthquake Eng. and Structural Dynamics*, *25*, 269-290.

18. Mulhern, M.R., and Maley, R.P. (1973). Building Period Measurements Before, During And After the San Fernando, California, Earthquake of February 9, 1971, *U.S. Depart. Of Commerce, National Oceanic and Atmospheric Administration,* Washington D.C., Vol. I, Part B, 725–733.

19. Todorovska, M.I., and Trifunac, M.D. (2006a). Damage detection in the Imperial County Services Building I: The data and time-frequency analysis, *Soil Dynamics and Earthquake Eng*., (in press).

20. Todorovska, M.I., and Trifunac, M.D. (2006b). Damage detection in the Imperial County Services Building II: Analysis of novelties via wavelets (submitted for publication).

21. Todorovska, M.I., and Trifunac, M.D. (2006c) Earthquake damage detection in the imperial county services building III: Analysis of wave travel times via impulse response functions (submitted for publication).

22. Todorovska, M.I., and Trifunac, M.D. (2006d). Impulse response analysis of the Van Nuys 7-story hotel during 11 earthquakes (1971-1994): one-dimensional wave propagation and inferences on global and local reduction of stiffness due to earthquake damage, Report CE 06-01, Dept. of Civil Eng., University of Southern California, Los Angeles, California.

23. Todorovska, M.I., Ivanović, S.S., and Trifunac, M.D. (2001a). Wave propagation in a seven-story reinforced concrete building: I. Theoretical models, *Soil Dynam. and Earthquake Engrg*, *21*(3), 211–223.

24. Todorovska, M.L, Ivanović, S.S., and Trifunac, M.D. (2001b). Wave propagation in a seven-story reinforced concrete building: II. Observed wavenumbers, *Soil Dynam. and Earthquake Engrg*, *21*(3), 225–236.

25. Trifunac, M.D., and Hao, T.Y. (2001c). 7-Story Reinforced Concrete Building in Van Nuys, California: Photographs of the Damage from the 1994 Northridge Earthquake, Dept. of Civil Eng. Report No. CE 01-05. Univ. of Southern California, Los Angeles, California.

26. Trifunac, M.D., and Ivanovic, S.S. (2003). Analysis of Drifts in a Seven-Story Reinforced Concrete Structure, *Dept. of Civil Eng. Report No. CE 03-01*, Univ. of Southern California, Los Angeles, California.

27. Trifunac, M.D., and Todorovska, M.I. (1998). "Damage distribution during the 1994 Northridge, California, earthquake in relation to generalized categories of surface geology", *Soil Dynam. and Earthquake Engrg, 17*(4), 238-252.

28. Trifunac, M.D., Ivanović, S.S., Todorovska, M.I., Novikova, E.I., and Gladkov, A.A. (1999a). Experimental evidence for flexibility of a building foundation supported by concrete friction piles, *Soil Dynam. and Earthquake Eng*., *18*, 169–187.

29. Trifunac, M.D., Ivanović, S.S., and Todorovska, M.I. (1999b). Seven-Story Reinforced Concrete Building in Van Nuys, California: strong Motion Data Recorded Between 7 Feb. 1971 and 9 Dec., 1994, and Description of Damage Following Northridge 17 January 1994 Earthquake, *Dept. of Civil Eng. Rep. CE 99-02*, Univ. of Southern California, Los Angeles, California.

30. Trifunac, M.D., Ivanović, S.S., and Todorovska, M.I. (2001a). Apparent periods of a building, Part I: Fourier analysis, *J. Struct. Engrg, ASCE*, *127*(5), 517–526.

31. Trifunac, M.D., Ivanović, S.S., and Todorovska, M.I. (2001b). Apparent periods of a building, Part II: Time-frequency analysis, *J. Struct. Engrg, ASCE*, *127*(5), 527–537.

32. Trifunac, M.D., Hao, T.Y. and Todorovska, M.I. (2001c). On energy flow in earthquake response, Dept. of Civil Engrg., Report CE 01-03, Univ. of Southern California, Los Angeles, California.

33. Trifunac, M.D., Ivanović, S.S., and Todorovska, M.I. (2003). Wave propagation in a seven-story reinforced concrete building III: Damage detection via changes in wave numbers. *Soil Dyn. and Earthquake Eng*., *23*(1), 65–75.